Applied Energy 229 (2018) 841–857

Contents lists available at ScienceDirect

Applied Energy

journal homepage: www.elsevier.com/locate/apenergy

A collaborative energy sharing optimization model among electric vehicle charging stations, commercial buildings, and power grid

Md Abdul Quddus*, Omid Shahvari, Mohammad Marufuzzaman, John M. Usher, Raed Jaradat

Department of Industrial & Systems Engineering, Mississippi State University, Mississippi State, MS 39762, United States

HIGHLIGHTS

- A collaborative decision model to study energy sharing among buildings and charging stations.
- A customized solution approach to solve the optimization model in a realistic-size problems.
- Managerial insights drawn for decision makers to design an efficient collaborative scheme.

ARTICLE INFO

Keywords:
Energy management
Stochastic optimization
Charging station
Vehicle-to-grid
Sample average approximation

ABSTRACT

This paper studied a collaborative decision model to optimize electricity flow among commercial buildings, electric vehicle (EV) charging stations, and the grid under power demand uncertainty. We propose a two-stage stochastic programming model that realistically captures different operational constraints between multiple commercial buildings and EV charging stations. We developed a customized solution approach based on Sample Average Approximation method that can solve the proposed model efficiently and accurately. Finally, a real-life case study is constructed that draws managerial insights into how different key input parameters (e.g., grid power unavailability, power collaboration restriction) affect the overall energy network design and cost.

1. Introduction

Commercial buildings and surface transportation sectors utilize a significant portion of energy causing a number of global challenges such as climate change and resource scarcity. According to the U.S. Energy Information Administration [1], buildings and surface transportation sectors consume approximately 43.35% and 28.79% of total energy generated in the United States, respectively. Regarding indirect emissions, both sectors cause approximately 78.9% of greenhouse gas (GHG) emissions, of which the building and transportation sectors are responsible for 44.6% and 34.3%, respectively [2]. Recently, the growing concerns of energy efficiency, dependence on fossil fuels, and environmental impacts have attracted increasing attention on smart buildings and electric vehicles (EVs) in relation to commercial building and road transportation sectors, respectively.

A *smart building* is a structure utilizing automated processes to control the building's operations including heating, ventilation, air conditioning, lighting, security, and other systems. According to [3], an undeniable fact about smart building management is the need to accurately coordinate its electrical and thermal loads. To achieve greater economic performance and environmental sustainability, an efficient energy management system is needed, which can optimally coordinate the generation, consumption, and storage of energy across the available resources [4,5]. On the other hand, *electric vehicle* sales in the U.S. increased by 22% from 2015 to 2016 and it is anticipated that there will be approximately 2.7 million EVs on the U.S. road by 2020 [6]. Furthermore, it is expected that the EV market share will hit 10% by 2025 [6]. Higher EV market penetration brings both challenges and opportunities in the area of power grid management. Unmanaged charging of EVs might trigger an extreme swell in electricity demand at peak hours and, consequently, negatively affect the stability and security of the power grid. This being the case, there is an urgent need to manage EV charging activity efficiently to promote widespread adoption of EVs. Towards this goal, this study investigates optimal operational strategies in relation to smart commercial buildings and electric vehicle charging stations to optimize individual and integrated operations under systems uncertainty.

The power grid is currently experiencing a variety of challenges

* Corresponding author.
E-mail addresses: mq90@msstate.edu (M.A. Quddus), shahvari@ise.msstate.edu (O. Shahvari), maruf@ise.msstate.edu (M. Marufuzzaman), usher@ise.msstate.edu (J.M. Usher), jaradat@ise.msstate.edu (R. Jaradat).

https://doi.org/10.1016/j.apenergy.2018.08.018
Received 9 May 2018; Received in revised form 24 July 2018; Accepted 4 August 2018
0306-2619/

from the viewpoint of sustainable development of advanced technologies. The future power grid, known as the *smart grid*, together with smart commercial buildings defines the next-generation of electrical power generation and consumption systems. The smart grid can be characterized by increased utilization of real time communications, information technology, and control and management in the production, distribution, and consumption of electrical energy. The aim of employing an upgraded smart grid together with smart commercial buildings is to allow two-way electricity and information flow between them so that they are capable of monitoring and responding to demand changes.

One possible way to alleviate excessive loads on the power grid is to design EV charging stations that integrate renewable energy resources (RES) with vehicle-to-grid (V2G) resources, while planning optimal charging schedules for EVs. A stream of studies have addressed the integration of the RES with V2G. Liu et al. [7] and Marmaras et al. [8] study the effects of EV smart charging patterns on power system scheduling, while considering coordination of wind energy, thermal units, and V2G. Likewise, He et al. [9] present a global and local scheduling model that is capable of making charging and discharging decisions for EVs with the goal of minimizing the overall system cost. Another study, proposed by Ortega et al. [10], integrates V2G with power systems in order to achieve better efficiency and security while operating under an existing power infrastructure. Along the same line, Haddadian et al. [11,12] study the effects of considering V2G and RES as viable resources for the smart grid. Similarly, Fathabadi [13] studies the different effects of incorporating V2G and RES in a power network. The goal is to identify the best coordination that is effective in sustaining the system while reducing cost and loss of power production. Thomas et al. [14] investigate the bi-directional capabilities of EV energy trading with respect to renewable power uncertainty. In another study, DeForest et al. [15] show a day-ahead optimization of an EV fleet providing ancillary services at the Los Angeles Air Force Base vehicle-to-grid demonstration, including a number of practical considerations and scenario analysis. Jin et al. [16] and Hong et al. [17] propose a stochastic optimization model to minimize the average cost of utilizing RES under system uncertainty. Rahmani-Andebili and Fotuhi-Firuzabad [18] propose a stochastic predictive control model for management charging of plug-in EVs and distribution system reconfigurations considering driving patterns of the plug-in EV owners. Another study, conducted by Zhang et al. [19], introduces a scheduling model to minimize the mean waiting time for charging electric vehicles at EV charging stations equipped with multiple plug outlets and the availability of RES. The authors consider arrival time of EVs, fluctuation in grid power prices, and the RES generation level using a markov decision process (MDP). The existing studies provided along this line attempt to manage operational decisions for a single charging station while no consideration is given to optimize integration decisions on cluster-based EV charging stations.

Several studies attempt to optimize battery management related decisions at battery swapping stations where an EV can quickly exchange its depleted battery with a fully-charged battery. Pan et al. [20] present a two-stage stochastic programming model to determine the optimal location of battery swapping stations and then make appropriate operational decisions (e.g., the number of charged and discharged batteries) based upon realized battery demands, EV loads, and production of RES energies. It can be note that decisions involving discharging batteries to the power grid during peak hours is an important feature of the proposed model. Similarly, Worley and Klabjan [21] present a dynamic programming model to determine the number of batteries purchased and their charging times based on dynamic changes in the power grid pricing rate. Along the same line, Mak et al. [22] propose various models that aid the planning process for establishing battery swapping infrastructure based on a robust optimization framework under demand uncertainty. The authors determine the potential impact of battery standardization and other related technology advancements on the optimal infrastructure establishment strategy. Nurre et al. [23] develop an integer programming model to determine the optimal operational decisions (e.g., the number of charged, discharged, and exchanged batteries) of a battery swapping station over a pre-specified planning horizon. Liu et al. [24,25] propose an optimization model to determine energy exchange strategies of a battery swapping station considering solar energy availability and demand management decisions (e.g., optimal pricing, charging and discharging batteries). Recently, Widrick et al. [26] demonstrate optimal policies for battery swapping station management, integrated with V2G capability, to control charging and discharging operations under non-stationary stochastic demand. Note that most of the existing studies provided along this line attempt to optimize battery management decisions (e.g., hourly charging, discharging, storing, and exchanging) within a single facility while no consideration is given to the integration between battery swapping and EV charging across multiple charging stations.

In addition to power grid load reduction and EV charging station management, another possible way to reduce the energy consumption from the two main sectors (i.e., commercial buildings and surface transportation) is via vehicle-to-building (V2B) connection capability. In the V2B integration mode, a smart commercial building can cooperate with an EV charging station(s) to achieve higher energy efficiency and lower network costs. This being the case, two-way electricity flow among related buildings and charging stations can help manage demand fluctuations. Flores et al. [27] show that significant cost savings cost be achieved if a charging station can be integrated with a commercial or industrial building using a coordinated operation strategy. Karan et al. [28] investigate possible GHG emission reduction and mitigation strategies based on the current trend of energy usage in transportation and building sectors. In another study, Clarke et al. [29] and Stadler et al. [30] demonstrate how the design of distributed energy systems can be improved by increasing participation of EVs battery storage, which enhances system flexibility and facilitates integration of further distributed energy resources such as solar and wind energy. Pang et al. [31] and Su et al. [32] demonstrate that V2B connections provide some benefits including backup power, high power quality for buildings, and peak shaving in the power grid. Additionally, the authors state that V2B integration can significantly improve demand side management and power outage. Gough et al. [33] find that participating in both the peak power and the ancillary services market may prove the most profitable for V2B connections. Sehar et al. [34] and Liu et al. [35] propose a heuristic operation strategy for a commercial building microgrid, equipped with EVs and a photovoltaic (PV) system, to improve self-consumption capability of PV energy. Erdinc [36] considers both pricing scheme and peak power limiting on demand response, which can further improve the economic advantage of the home energy management structure by increasing flexibility. Studies by [37–39] investigate the impact of integrating the EVs into an office building microgrid, which is supported by PV and combined heat and power (CHP) units. Authors found that the EVs with optimal coordinated charging strategies can help in reducing the fluctuation grid energy during the peak hours. Recently, Robledo et al. [40] study the performance of an integrated hydrogen fuel cell EV with V2G technology, PV power, and a residential building. The results show that integrated model can reduce imported electricity from the power grid by approximately 71%.

To the best of the author's knowledge, none of the prior studies have investigated the effects that integrated cluster-based smart commercial buildings and EV charging stations will have on operational decisions under uncertainty. To fill this gap in the literature, this study proposes a novel collaborative energy sharing decision model to study energy sharing among a cluster of commercial buildings and EV charging stations in concert with the power grid. In summary, the main contributions of this paper to the existing literature are summarized as follows:

- Investigating the effects of integrated cluster-based smart commercial buildings and EV charging stations on the overall system performance under power demand uncertainty.
- Proposing a novel collaborative energy sharing decision model which realistically captures the operational constraints for different viable resources used in both commercial buildings (e.g., combined cooling, heating, and power (CCHP) system, renewable energy) and EV charging stations (e.g., renewable energy, V2G, battery swapping capability).
- Implementing a customized solution approach where the performance of the basic Sample Average Approximation (SAA) algorithm is enhanced by adding some problem-specific valid inequalities to solve our proposed optimization model in a large scale problem setting.
- Constructing a real-world case study to test the performance of the algorithms and reveal interesting managerial insights. We demonstrate the computational performance of our customized hybrid algorithm relative to its generic version. We use San Francisco, California as a testing ground to visualize and validate the modeling results. The outcome of this study provides a number of managerial insights, such as the impact of demand variability, grid power disruption, power collaboration limit, and renewable energy cell sizes on overall system performance, which can effectively aid decision makers to design a cost-efficient collaborative system between multiple commercial buildings and EV charging stations.

An outline of this paper is as follows. Section 2 introduces the network structure, the problem description, and the model formulation. A customized solution approach to solve the proposed mathematical model is then presented in Section 3. The first part of Section 4 describes the input parameters used to construct the real-life case study while the second and third part represent, respectively, the performance of the customized solution approach and sensitivity analysis results. Finally, Section 5 concludes our study by summarizing the key managerial insights obtained from this study and offers possible future research directions.

2. Problem description and model formulation

In this section, we first specify the network structure of the proposed collaborative energy system consisting of EV charging stations, commercial buildings, and a power grid. Next, a mixed-integer linear programming (MILP) model is proposed to determine the optimal configuration between the energy sharing system under power demand uncertainty. It is worth noting that the MILP model is proposed from a system operator point of view for both commercial buildings and EV charging stations. To the end of this section, few problem specific valid inequalities are proposed to accelerate the computational performance of the proposed optimization model.

2.1. Network structure

The electricity, cooling, and heating demands of a commercial building and electricity demand of an EV charging station are primarily supplied from a variety of internal and external energy sources. Internal energy sources of a commercial building include but not limited to renewable energy resources (RES), a thermal energy storage (TES), a combined cooling, heating, and power (CCHP) system (consisting of a power generation unit (PGU), a heat recovery subsystem (HRS), an absorption chiller, and a heating exchanger), a battery storage (typically known as *commercial-grade battery*), and an auxiliary boiler. Likewise, internal energy sources of an EV charging station include the RES, vehicle-to-grid (V2G), and swappable batteries. The external energy sources for both commercial buildings and EV charging stations are the power grid and the entities itself for each other (e.g., EV charging station can exchange electricity with commercial buildings and vice versa). Each EV charging station can be connected with one or more commercial buildings and vice versa while it is assumed that both are connected with one power grid. Fig. 1 provides a simple illustration of energy collaboration between a power grid, a commercial building, and an EV charging station.

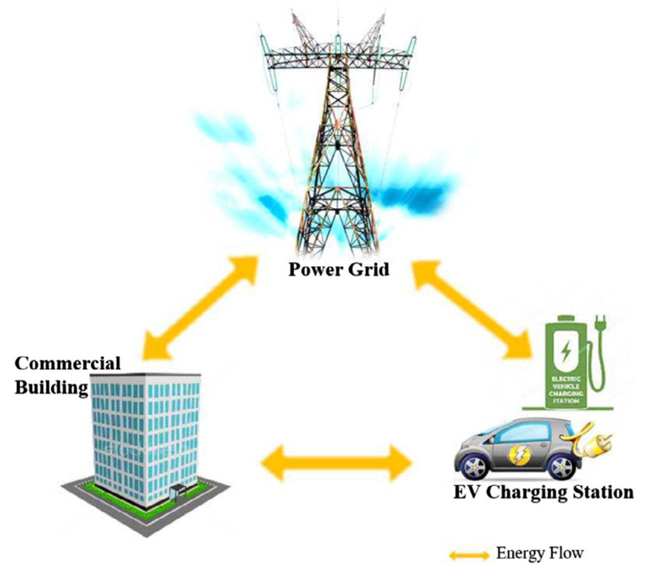

Fig. 1. A simple illustration of two-way energy collaboration between different network entities.

In relation to a commercial building, the PGU supplies a significant portion of electricity demand for the buildings while the surplus energy is stored at a commercial-grade battery. Additionally, the PGU is capable of supplying thermal energy to fulfill thermal demand for the buildings. This is primarily due to the fact that the required thermal energy of a commercial building may not be satisfied only via an auxiliary boiler due to its limited supply capacity. Further, we note that the thermal load requirements of a building is fulfilled from the waste heat of the PGU recovered through the HRS in the CCHP system and/or an auxiliary boiler. The auxiliary boiler converts fuel into heat to compensate the possible shortage of thermal load on the building. An absorption chiller and a heating exchanger are used as the cooling and heating components (referred to as CC and HC, respectively) in the CCHP system, while surplus thermal energies from both the PGU and the auxiliary boiler are stored at the TES. Therefore, commercial-grade battery and the TES have the capability to control any fluctuation that results due to the stochasticity in the prime mover.

In relation to charging stations, electric vehicles have options either to swap their batteries or charge through charging stations. As shown in Fig. 1, both commercial buildings and EV charging stations are connected with a power grid which supplies the electricity load requirements for the facilities. If the entities are unable to support each other, then the power demand for the buildings and the charging stations can be supplied from the main grid. In case if none of the sources are capable of supplying energy demand for the buildings and the charging stations (i.e., an extreme scenario such as hurricane), we assume that the facilities still can satisfy the unmet energy demand via an external energy source(s) by paying a high penalty cost. However, if the facilities produce additional energy, they have the option to sell these energy back to the grid or between each other which thereby can be treated as an additional source of income for the facilities. Fig. 2 demonstrates the structure and energy flow among different network entities along with components of each facility.

2.2. Problem description

In this section, we present a two-stage stochastic mixed-integer

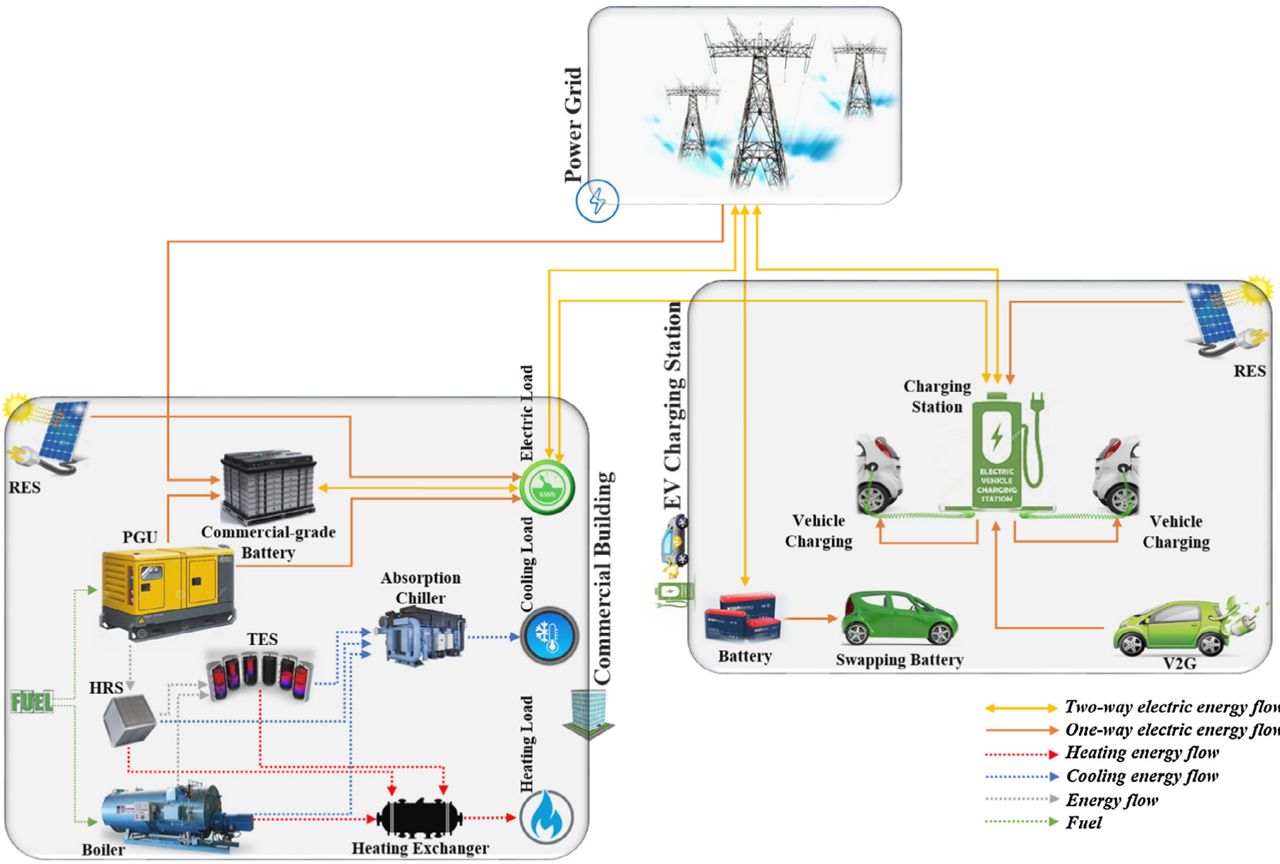

Fig. 2. Network illustration of energy flow among commercial buildings, EV charging stations, and grid.

programming (MIP) formulation that minimizes the operational and collaboration cost among a set of commercial buildings $\mathscr{B} = \{1, 2, ..., B\}$, EV charging stations $\mathscr{I} = \{1, 2, ..., I\}$, and power grid over a pre-specified planning horizon $\mathscr{T} = \{1, 2, ..., T\}$. Due to sparse location of the facilities, we denote $\mathscr{I}_b \subset \mathscr{I}$ to be the subset of charging stations that are connected with a commercial building $b \in \mathscr{B}$ while $\mathscr{B}_i \subset \mathscr{B}$ to represent the vice versa. The operational decisions of a commercial building $b \in \mathscr{B}$ include energy flow via the CCHP system, the RES, the TES, the boiler, and the commercial-grade battery. Further, the decisions involving the number of batteries stored, charged, discharged, and exchanged as well as the energy flow through V2G and the RES are considered as the operational decisions for an EV charging station $\mathscr{I}$.

Electricity demand for commercial buildings and charging stations cannot be accurately predicted in advance. Let Ω be the set of scenarios of different realization of power demand for the commercial buildings and EV charging stations where $\omega \in \Omega$ defines a particular realization and $\sum_{\omega\in\Omega} \rho_\omega = 1$. Let $d_{bt\omega}$ be the total demand load in commercial building $b \in \mathscr{B}$ at time period $t \in \mathscr{T}$ under scenario $\omega \in \Omega$. We further denote $\lambda\delta_{t\omega}f_{it}$ be the power demand for each charging station $i \in \mathscr{I}$ which can be determined based on an assumption that $\delta_{t\omega}$ percentage of the total EVs f_{it} passes through the charging station $i \in \mathscr{I}$ at time period $t \in \mathscr{T}$ may require charging while λ denote average unit power required to charge each electric vehicle (*kWh*). In [41,42], the behavioral of PEVs drivers are modeled with respect to the value of incentive, the distance from the parking lot, and aggregator's viewpoint. In this study, we first identified existing EV charging stations on target area, denoted as a set *I*. Then, we define f_{it} as the number of EVs passing through the charging station $i \in \mathscr{I}$ at time period $t \in \mathscr{T}$. Estimating f_{it} is a challenging problem, and it can be even more difficult depending upon traffic and road geometry (e.g., curvy links). A rough estimation of f_{it} is obtained by developing a routing algorithm that deploys EVs from multiple sources to destination points in order to get an estimation of the number of vehicles, which are passed through each link of the real-world physical network [43]. Depending on the fluctuations in energy demand, commercial buildings and charging stations may exchange energy between them. We now make the following assumptions to simplify our modeling approach without the loss of generality:

Assumption 1. Limited energy flow from/to power grid to/from commercial buildings and EV charging stations and between commercial buildings and EV charging stations.

Assumption 2. Maximum and minimum rate of charging/discharging and SoC[1] level for commercial-grade battery/TES.

Assumption 3. Limited storage availability and plug-ins for charging/discharging of the batteries in an EV charging station

2.3. Model formulation

Let us now summarize the following notation for our proposed two-stage stochastic programming model formulation. Note that we introduce parameters by *lowercase and Greek letters* while decision variables as *uppercase letters*. Additionally, the superscript and subscript of a parameter and decision variable represent their *brief descriptions* and *indices*, respectively.

Sets and Indices:

- $\mathscr{B}$: set of commercial buildings, indexed by b
- $\mathscr{I}$: set of EV charging stations, indexed by i
- $\mathscr{T}$: set of time periods, indexed by t

[1] Refers to *state of charge* which is the ratio of available energy to the maximum storage energy in commercial-grade battery/TES.

- Ω: set of scenarios, indexed by ω

Subsets:

- $\mathscr{I}_b$: subset of EV charging stations associated with commercial building b, $\mathscr{I}_b \subset \mathscr{I}$
- $\mathscr{B}_i$: subset of commercial buildings associated with EV charging station i, $\mathscr{B}_i \subset \mathscr{B}$

For the sake of simplicity, in the definitions of parameters and decision variables, commercial buildings and EV charging stations are referred to as just *buildings* and *charging stations*, respectively.

Commercial Building Parameters:

- ψ_b^{pgu}/ψ_b^{bo}: PGU/boiler startup cost in building b
- s_b^{pgu}/s_b^{bo}: PGU/boiler fuel consumption capacity in building b
- η^{pgu}/η^{bo}: PGU/boiler system efficiency
- c^f: unit fuel price for PGU/boiler ($\$/gl.$)
- a^{pgu}, b^{pgu}: PGU electricity generation efficiency
- a_b: RES size in building b
- $d_{bt\omega}$: total demand load in building b in time period t under scenario ω
- $\pi_t^e/\pi_t^c/\pi_t^h$: percentage of total demand load for electric demand/cooling/heating in time period t
- η^{cb}/η^{db}: commercial-grade battery charging/discharging efficiency
- η^{ce}/η^{de}: TES charging/discharging efficiency
- η^{cc}/η^{hc}: CC/HC efficiency
- b_{bt}^{bp}: availability of grid power for building b in time period t
- b_{bt}^{bn}: maximum power flow to PG from building b in time period t
- $\overline{q}^{b+}/\underline{q}^{b+}$: maximum/minimum percentage of commercial-grade battery charging capacity
- $\overline{q}^{b-}/\underline{q}^{b-}$: maximum/minimum percentage of commercial-grade battery discharging capacity
- $\overline{q}^{e+}/\underline{q}^{e+}$: maximum/minimum percentage of TES charging capacity
- $\overline{q}^{e-}/\underline{q}^{e-}$: maximum/minimum percentage of TES discharging capacity
- s_b^{bs}/s_b^{tes}: commercial-grade battery/TES capacity in building b
- $s_{bt}^{bs+}/s_{bt}^{bs-}$: maximum/minimum SoC of commercial-grade battery in building b in time period t
- $s_{bt}^{tes+}/s_{bt}^{tes-}$: maximum/minimum SoC of TES in building b in time period t
- s_{b0}^{bs}: initial SoC of commercial-grade battery in building b
- s_{b0}^{tes}: initial SoC of TES in building b

EV Charging Station Parameters:

- c_t^{v2g}: unit V2G electricity energy cost in time period t ($\$/kWh$)
- c_t^s: unit battery storage cost in time period t
- a_i: RES size in charging station i
- u_i: maximum availability of batteries in charging station i
- b_{it}^{cp}: availability of grid power for charging station i in time period t
- b_{bt}^{bn}: maximum power that can be flowed to PG from charging station i in time period t
- λ: average unit power required to charge each electric vehicle (kWh)
- γ: average unit power obtained from discharging each electric vehicle (kWh)
- q_i^{in}/q_i^{out}: number of plug-ins available for charging/discharging batteries in charging station i
- f_{it}: electric vehicle flow around charging station i in time period t
- $\delta_{t\omega}$: percentage of electric vehicles charged at an EV charging station in time period t under scenario ω
- β_t: percentage of electric vehicles discharged at an EV charging station in time period t

Other Parameters:

- g_t^{pg}: overall grid power availability in time period t
- g_t^{bp}/g_t^{cp}: available grid power for buildings/charging stations in time period t
- χ_{bit}^{bc}: maximum power that can flow from building b to charging station i in time period t
- χ_{ibt}^{cb}: maximum power that can flow from charging station i to building b in time period t
- c_t^+: unit electricity purchasing price from power grid in time period t ($\$/kWh$)
- c_t^-: unit electricity selling price to power grid in time period t ($\$/kWh$)
- c_t^t: unit electricity transaction price among any pair of building and charging station in time period t ($\$/kWh$)
- c_t^{us}: unit penalty cost for power shortage in time period t ($\$/kWh$)
- γ^c: carbon emission tax
- ν^{etc}: electricity-to-carbon conversion factor
- ν^{ftc}: fuel-to-carbon conversion factor
- μ_t: solar radiation in time period t
- η^{rr}: RES electricity generation efficiency
- τ: energy conversion factor (kWh to Btu)
- ρ_ω: probability of scenario ω

In the following, the first- and second-stage decision variables associated with commercial buildings and EV charging stations for our proposed two-stage stochastic mixed-integer linear programming model are briefly explained.

Commercial Building Decision Variables:
First-stage Decision Variables:

- Z_{bt}^p: 1 if PGU state is *on* in building b at time period t; 0 otherwise
- Z_{bt}^b: 1 if boiler state is *on* in building b at time period t; 0 otherwise
- S_{bt}^{e+}: 1 if TES charging state is *on* in building b at time period t; 0 otherwise
- S_{bt}^{e-}: 1 if TES discharging state is *on* in building b at time period t; 0 otherwise
- S_{bt}^{b+}: 1 if commercial-grade battery charging state is *on* in building b at time period t; 0 otherwise
- S_{bt}^{b-}: 1 if commercial-grade battery discharging state is *in* at building b in time period t; 0 otherwise
- Y_{bt}^{p+}: 1 if electricity transaction state from power grid is *on* in building b at time period t; 0 otherwise
- Y_{bt}^{p-}: 1 if electricity transaction state to PG is *on* in building b at time period t; 0 otherwise
- Y_{bit}^{s+}: 1 if electricity transaction state to charging station i is *on* in building b at time period t; 0 otherwise

Second-stage Decision Variables:

- $H_{bt\omega}^+$: electricity flow from power grid to building b in time period t under scenario ω
- $H_{bt\omega}^-$: electricity flow from building b to power grid in time period t under scenario ω
- $X_{bt\omega}^{pb}$: electricity flow from PGU to commercial-grade battery in building b at time period t under scenario ω
- $X_{bt\omega}^{gb}$: electricity flow from power grid to commercial-grade battery in building b at time period t under scenario ω
- $M_{bit\omega}^+$: electricity flow from building b to charging station i at time period t under scenario ω
- $Z_{bt\omega}^{brr}$: Electricity generated in RES at building b in time period t under scenario ω
- $X_{bt\omega}^{pgu}$: Electricity generated in PGU at building b in time period t

under scenario ω
- $U^{bd}_{bt\omega}$: power shortage in building b at time period t under scenario ω
- $B^{bd}_{bt\omega}$: PGU fuel consumed in building b at time period t under scenario ω
- $B^{bo}_{bt\omega}$: boiler fuel consumed in building b at time period t under scenario ω
- $X^{cb}_{bt\omega}$: electricity flow from building b to its commercial-grade battery at time period t under scenario ω
- $X^{db}_{bt\omega}$: electricity flow to building b from its commercial-grade battery at time period t under scenario ω
- $X^{b}_{bt\omega}$: commercial-grade battery stored electricity in building b at time period t under scenario ω
- $X^{e}_{bt\omega}$: TES stored thermal energy in building b at time period t under scenario ω
- $X^{ce}_{bt\omega}$: thermal energy charged in building b at time period t under scenario ω
- $X^{de}_{bt\omega}$: thermal energy discharged in building b at time period t under scenario ω
- $Q^{cc}_{bt\omega}$: thermal energy flow from HRS and boiler to CC in building b at time period t under scenario ω
- $Q^{sc}_{bt\omega}$: thermal energy flow from TES to CC in building b at time period t under scenario ω
- $Q^{ch}_{bt\omega}$: thermal energy flow from HRS and boiler to HC in building b at time period t under scenario ω
- $Q^{sh}_{bt\omega}$: thermal energy flow from TES to HC in building b at time period t under scenario ω
- $Q^{cs}_{bt\omega}$: thermal energy flow from HRS and boiler to TES in building b at time period t under scenario ω

EV Charging Station Decision Variables:
First-stage Decision Variables:

- Y^{c+}_{it}: 1 if battery charging state is *on* in charging station i at time period t; 0 otherwise
- Y^{c-}_{it}: 1 if battery discharging state is *on* in charging station i at time period t; 0 otherwise
- Y^{p+}_{it}: 1 if electricity transaction state from power grid is *on* in charging station i at time period t; 0 otherwise
- Y^{p-}_{it}: 1 if electricity transaction state to power grid is *on* in charging station i at time period t; 0 otherwise
- Y^{s-}_{ibt}: 1 if electricity transaction state to building b is *on* in charging station i at time period t; 0 otherwise

Second-stage Decision Variables:

- $G^{+}_{it\omega}$: electricity flow from power grid to charging station i at time period t under scenario ω
- $G^{-}_{it\omega}$: electricity flow from charging station i to power grid at time period t under scenario ω
- $V_{it\omega}$: electricity flow from V2G to charging station i at time period $t \in \mathscr{T}$ under scenario ω
- $M^{-}_{ibt\omega}$: electricity flow from charging station i to building b at time period t under scenario ω
- $U^{cs}_{it\omega}$: power shortage in charging station i at time period t under scenario ω
- $Z^{crr}_{it\omega}$: RES generated electricity in charging station i at time period t under scenario ω
- $B_{it\omega}$: number of batteries swapped in charging station i at time period t under scenario ω
- $W_{it\omega}$: number of fully-charged batteries available in charging station i at time period t under scenario ω
- $S_{it\omega}$: number of batteries charged in charging station i at time period t under scenario ω
- $P_{it\omega}$: number of batteries discharged in charging station i at time period t under scenario ω

The objective of model **[BEV]** is to minimize the first-stage and the expected value of the random second-stage costs across all possible electricity demand scenarios. Electricity demand for commercial buildings and charging stations cannot be accurately predicted in advance. Therefore, the electricity demand is modeled as a random variable of which probability distribution may not be known in advance. Thus, a set of scenarios Ω of different realization of power demand for the commercial buildings and EV charging stations is defined, where each scenario $\omega \in \Omega$ is associated with a positive probability ρ_ω ($\sum_{\omega\in\Omega}\rho_\omega = 1$). It is important to note that, the first-stage minimizes the costs associated with PGU and boiler startup prior to the realization of any stochastic event (e.g., electricity demands for commercial buildings and charging stations). However, after the uncertainty is revealed, the second-stage decisions are made which include operational decisions in the commercial buildings (e.g., thermal management decisions), charging stations (e.g., battery management decisions), and the collaboration between them and grid. These decisions depend on the first-stage decisions which are made after the uncertainties are unveiled and pertain to the real-time operation. In the following, the proposed two-stage stochastic mixed-integer linear programming model, referred to as **[BEV]**, is provided.

$$
\begin{aligned}
\textbf{[BEV]}\ Min\ & \underbrace{\sum_{t\in\mathscr{T}}\left(\sum_{b\in\mathscr{B}}(\psi^{pgu}_b Z^p_{bt} + \psi^{bo}_b Z^b_{bt})\right)}_{\text{First-stage startup cost}} \\
& - \sum_{t\in\mathscr{T}}\sum_{\omega\in\Omega}\rho_w\left\{\underbrace{\sum_{b\in\mathscr{B}} c^-_t H^-_{bt\omega} + \sum_{i\in\mathscr{I}}(c^-_t G^-_{it\omega} + \gamma c^-_t P_{it\omega})}_{\text{Second-stage building and charging station benefit}}\right. \\
& + \underbrace{\sum_{b\in\mathscr{B}}\left(c^+_t H^+_{bt\omega} + \gamma^c\nu^{etc} H^+_{bt\omega} + c^{us}_t U^{bd}_{bt\omega} + c^+_t X^{gb}_{bt\omega} + c^t_t\sum_{i\in\mathscr{I}_b} M^-_{ibt\omega}\right)}_{\text{Second-stage commercial building electricity cost}} \\
& + \underbrace{\sum_{b\in\mathscr{B}}(c^f B^{bd}_{bt\omega} + \gamma^c\nu^{ftc} B^{bd}_{bt\omega} + c^f B^{bo}_{bt\omega} + \gamma^c\nu^{ftc} B^{bo}_{bt\omega})}_{\text{Second-stage commercial building thermal energy cost}} \\
& + \underbrace{\sum_{i\in\mathscr{I}}\left(c^+_t G^+_{it\omega} + \gamma^c\nu^{etc} G^+_{it\omega} + \gamma^c\nu^{etc} S_{it\omega} + c^{v2g}_t V_{it\omega} + c^{us}_t U^{cs}_{it\omega} + c^t_t\sum_{b\in\mathscr{B}_i} M^+_{bit\omega}\right)}_{\text{Second-stage EV charging station electricity cost}} \\
& \left. + \underbrace{\sum_{i\in\mathscr{I}}(\lambda c^+_t S_{it\omega} + c^s_t W_{it\omega})}_{\text{Second-stage EV charging station battery cost}}\right\}
\end{aligned}
$$

In **[BEV]**, the first-stage represents the costs associated with PGU and boiler startup, while the second-stage represents the costs associated with commercial buildings electricity and thermal energy management costs, EV charging stations electricity and battery management costs, and the benefits associated with selling/discharging electricity to power grid by the commercial buildings and EV charging stations, respectively. Electricity cost of a commercial building $b \in \mathscr{B}$ represents the costs associated with electricity flow to that building from the power grid, connected EV charging stations, RES, PGU, and commercial-grade batteries. On the other hand, thermal cost represents the costs associated with thermal flow to the heating and cooling components which are obtained from the HRS, boiler, and TES of a commercial building $b \in \mathscr{B}$. Similarly, costs associated with electricity flow (e.g., from V2G, power grid, RES, and commercial buildings) and battery charging/discharging/storing are considered as electricity cost and battery management cost for an EV charging station $i \in \mathscr{I}$, respectively.

Constraints associated with commercial buildings:

Constraints for Electric Load Balance: Constraints (1) ensure that the power demand for commercial building $b \in \mathscr{B}$ at time period $t \in \mathscr{T}$ and under scenario $\omega \in \Omega$ can be satisfied via grid, RES, commercial-grade battery, PGU, EV charging station, and an external source(s) to compensate power shortage. Note that the surplus electricity can be sold back to the grid or to the EV charging stations or stored them on the commercial-grade batteries at building $b \in \mathscr{B}$.

$$H^{+}_{bt\omega} + Z^{brr}_{bt\omega} + X^{pgu}_{bt\omega} + \eta^{db} X^{db}_{bt\omega} + \sum_{i \in \mathscr{I}_b} M^{-}_{ibt\omega} + U^{bd}_{bt\omega} = \pi^{e}_{t} d_{bt\omega} + H^{-}_{bt\omega} + \frac{X^{cb}_{bt\omega}}{\eta^{cb}} + \sum_{i \in \mathscr{I}_b} M^{+}_{bit\omega} \quad \forall\, b \in \mathscr{B},\ t \in \mathscr{T},\ \omega \in \Omega \tag{1}$$

Constraints (2) restrict electricity flow from a commercial building $b \in \mathscr{B}$ to an EV charging station $i \in \mathscr{I}$ at time period $t \in \mathscr{T}$ and under scenario $\omega \in \Omega$. Constraints (3) indicate that at any particular time period $t \in \mathscr{T}$ electricity can flow only one way between a commercial building $b \in \mathscr{B}$ and an EV charging station $i \in \mathscr{I}$.

$$M^{+}_{bit\omega} \leqslant \chi^{bc}_{bit} Y^{s+}_{bit} \quad \forall\, b \in \mathscr{B},\ i \in \mathscr{I},\ t \in \mathscr{T},\ \omega \in \Omega \tag{2}$$

$$Y^{s+}_{bit} + Y^{s-}_{ibt} \leqslant 1 \quad \forall\, b \in \mathscr{B},\ i \in \mathscr{I},\ t \in \mathscr{T} \tag{3}$$

Constraints for Thermal Energy Load Balance: Constraints (4) and (5) guarantee cooling and heating supply for cooling and heating loads of each building $b \in \mathscr{B}$ at time period $t \in \mathscr{T}$ under scenario $\omega \in \Omega$ based on thermal energy flow from the HRS, boiler, and the TES.

$$\eta^{cc}(Q^{cc}_{bt\omega} + Q^{sc}_{bt\omega}) = \tau \pi^{c}_{t} d_{bt\omega} \quad \forall\, b \in \mathscr{B},\ t \in \mathscr{T},\ \omega \in \Omega \tag{4}$$

$$\eta^{hc}(Q^{ch}_{bt\omega} + Q^{sh}_{bt\omega}) = \tau \pi^{h}_{t} d_{bt\omega} \quad \forall\, b \in \mathscr{B},\ t \in \mathscr{T},\ \omega \in \Omega \tag{5}$$

Constraints for RES: Constraints (6) indicate that the availability of renewable energy to a commercial building $b \in \mathscr{B}$ at time period $i \in \mathscr{T}$ and under scenario $\omega \in \Omega$ is restricted by the size of RES (a_b), electricity generation efficiency (η^{rr}), and the amount of solar radiation absorbed by the RES (μ_t).

$$Z^{brr}_{bt\omega} \leqslant a_b \mu_t \eta^{rr} \quad \forall\, b \in \mathscr{B},\ t \in \mathscr{T},\ \omega \in \Omega \tag{6}$$

Constraints for Commercial-grade Battery: This set of constraints (7)–(13) determine the states of commercial-grade battery for time period $t \in \mathscr{T}$ under scenario $\omega \in \Omega$. More specifically, constraints (7) indicate that a commercial-grade battery cannot be charged and discharged simultaneously in a given time period $t \in \mathscr{T}$. Constraints (8) restrict the electricity storage in a commercial-grade battery, while constraints (9) and (10) determine the battery energy stored at time period t based on the storage available at $t-1$ along with the energy charged or discharged at the batteries with respect to their charging and discharging rates. Constraints (11) and (12) restrict the amount of charged and discharged battery energy. Finally, constraints (13) determine the stored battery energy available at time period $t \in \mathscr{T}$ with respect to the energy obtained from the commercial building, PGU, and power grid.

$$S^{b+}_{bt} + S^{b-}_{bt} \leqslant 1 \quad \forall\, b \in \mathscr{B},\ t \in \mathscr{T} \tag{7}$$

$$s^{bs}_{b} s^{bs-}_{bt} \leqslant X^{b}_{bt\omega} \leqslant s^{bs}_{b} s^{bs+}_{bt} \quad \forall\, b \in \mathscr{B},\ t \in \mathscr{T},\ \omega \in \Omega \tag{8}$$

$$X^{b}_{b1\omega} - s^{bs}_{b} s^{bs}_{b0} = \frac{X^{cb}_{b1\omega}}{\eta^{cb}} - \frac{X^{db}_{b1\omega}}{\eta^{db}} \quad \forall\, b \in \mathscr{B},\ \omega \in \Omega \tag{9}$$

$$X^{b}_{bt\omega} - X^{b}_{b,t-1,\omega} = \frac{X^{cb}_{bt\omega}}{\eta^{cb}} - \frac{X^{db}_{bt\omega}}{\eta^{db}} \quad \forall\, b \in \mathscr{B},\ t \geqslant 2,\ t \in \mathscr{T},\ \omega \in \Omega \tag{10}$$

$$s^{bs}_{b} \underline{q}^{b+} S^{b+}_{bt} \leqslant \frac{X^{cb}_{bt\omega}}{\eta^{cb}} \leqslant s^{bs}_{b} \overline{q}^{b+} S^{b+}_{bt} \quad \forall\, b \in \mathscr{B},\ t \in \mathscr{T},\ \omega \in \Omega \tag{11}$$

$$s^{bs}_{b} \underline{q}^{b-} S^{b-}_{bt} \leqslant \frac{X^{db}_{bt\omega}}{\eta^{db}} \leqslant s^{bs}_{b} \overline{q}^{b-} S^{b-}_{bt} \quad \forall\, b \in \mathscr{B},\ t \in \mathscr{T},\ \omega \in \Omega \tag{12}$$

$$X^{b}_{bt\omega} = X^{pb}_{bt\omega} + X^{gb}_{bt\omega} + \frac{X^{cb}_{bt\omega}}{\eta^{cb}} \quad \forall\, b \in \mathscr{B},\ t \in \mathscr{T},\ \omega \in \Omega \tag{13}$$

Constraints for PGU and Boiler: Constraints (14) and (15) restrict the PGU and boiler fuel consumption with respect to their maximum capacities (s^{pgu}_{b} and s^{bo}_{b}). Constraints (16) ensure electricity flow to commercial-grade battery and corresponding building in terms of the PGU fuel consumption and electricity generation efficiency. Constraints (17) restrict thermal energy flow, generated by the PGU and boiler, to the heating and cooling components and TES. It is worth noting that the additional thermal energy is stored at the TES.

$$B^{bd}_{bt\omega} \leqslant s^{pgu}_{b} Z^{p}_{bt} \quad \forall\, b \in \mathscr{B},\ t \in \mathscr{T},\ \omega \in \Omega \tag{14}$$

$$B^{bo}_{bt\omega} \leqslant s^{bo}_{b} Z^{b}_{bt} \quad \forall\, b \in \mathscr{B},\ t \in \mathscr{T},\ \omega \in \Omega \tag{15}$$

$$X^{pb}_{bt\omega} + X^{pgu}_{bt\omega} = (B^{bd}_{bt\omega} - b^{pgu} Z^{p}_{bt})/a^{pgu} \quad \forall\, b \in \mathscr{B},\ t \in \mathscr{T},\ \omega \in \Omega \tag{16}$$

$$Q^{cs}_{bt\omega} + Q^{cc}_{bt\omega} + Q^{ch}_{bt\omega} \leqslant \eta^{pgu} B^{bd}_{bt\omega} + \eta^{bo} B^{bo}_{bt\omega} \quad \forall\, b \in \mathscr{B},\ t \in \mathscr{T},\ \omega \in \Omega \tag{17}$$

Constraints for TES: This set of constraints (18)–(25) determine the TES states for time period $t \in \mathscr{T}$ under scenario $\omega \in \Omega$. More specifically, constraints (18) indicate that the TES cannot be charged and discharged simultaneously in a particular time period $t \in \mathscr{T}$. Constraints (19) restrict the thermal energy storage in the TES, while constraints (20) and (21) determine thermal energy storage at time period t based on the storage available at $t-1$ along with the amount of thermal energy charged or discharged in that time period. Constraints (22) and (23) restrict the amount of charged and discharged TES thermal energy at each building $b \in \mathscr{B}$ in time period $t \in \mathscr{T}$. Constraints (24) indicate that the thermal energy passed to the heating and cooling components is restricted by the TES's discharging rate (η^{de}). Finally, constraints (25) indicate that thermal energy flow from the HRS and boiler to the TES is restricted by its charging rate (η^{ce}).

$$S^{e+}_{bt} + S^{e-}_{bt} \leqslant 1 \quad \forall\, b \in \mathscr{B},\ t \in \mathscr{T} \tag{18}$$

$$s^{tes}_{b} s^{tes-}_{bt} \leqslant X^{e}_{bt\omega} \leqslant s^{tes}_{b} s^{tes+}_{bt} \quad \forall\, b \in \mathscr{B},\ t \in \mathscr{T},\ \omega \in \Omega \tag{19}$$

$$X^{e}_{b1\omega} - s^{tes}_{b} s^{tes}_{b0} = \frac{X^{ce}_{b1\omega}}{\eta^{ce}} - \frac{X^{de}_{b1\omega}}{\eta^{de}} \quad \forall\, b \in \mathscr{B},\ \omega \in \Omega \tag{20}$$

$$X^{e}_{bt\omega} - X^{e}_{b,t-1,\omega} = \frac{X^{ce}_{bt\omega}}{\eta^{ce}} - \frac{X^{de}_{bt\omega}}{\eta^{de}} \quad \forall\, b \in \mathscr{B},\ t \geqslant 2,\ t \in \mathscr{T},\ \omega \in \Omega \tag{21}$$

$$s^{tes}_{b} \underline{q}^{e+} S^{e+}_{bt} \leqslant \frac{X^{ce}_{bt\omega}}{\eta^{ce}} \leqslant s^{tes}_{b} \overline{q}^{e+} S^{e+}_{bt} \quad \forall\, b \in \mathscr{B},\ t \in \mathscr{T},\ \omega \in \Omega \tag{22}$$

$$s^{tes}_{b} \underline{q}^{e-} S^{e-}_{bt} \leqslant \frac{X^{de}_{bt\omega}}{\eta^{de}} \leqslant s^{tes}_{b} \overline{q}^{e-} S^{e-}_{bt} \quad \forall\, b \in \mathscr{B},\ t \in \mathscr{T},\ \omega \in \Omega \tag{23}$$

$$Q^{sc}_{bt\omega} + Q^{sh}_{bt\omega} = \frac{X^{de}_{bt\omega}}{\eta^{de}} \quad \forall\, b \in \mathscr{B},\ t \in \mathscr{T},\ \omega \in \Omega \tag{24}$$

$$\frac{X^{ce}_{bt\omega}}{\eta^{ce}} = Q^{cs}_{bt\omega} \quad \forall\, b \in \mathscr{B},\ t \in \mathscr{T},\ \omega \in \Omega \tag{25}$$

Constraints associated with EV Charging Stations:

Constraints for Electric Load Balance: Constraints (26) ensure that the power demand for EV charging station $i \in \mathscr{I}$ at time period $t \in \mathscr{T}$ and under scenario $\omega \in \Omega$ can be satisfied via grid, V2G, batteries, commercial buildings, and an external source(s) to compensate power shortage. Note that the surplus electricity can be sold back to the grid or to the commercial buildings. The power demand for EV charging station $i \in \mathscr{I}$ at time period $t \in \mathscr{T}$ and under scenario $\omega \in \Omega$ can be determined based on electric vehicle flow (f_{it}), percentage of charged vehicles ($\delta_{t\omega}$), and average unit power required to charge each vehicle (λ).

$$G^{+}_{it\omega} + Z^{crr}_{it\omega} + \sum_{b \in \mathscr{B}_i} M^{+}_{bit\omega} + V_{it\omega} + \lambda B_{it\omega} + U^{cs}_{it\omega} = \lambda \delta_{t\omega} f_{it} + \sum_{b \in \mathscr{B}_i} M^{-}_{ibt\omega} + G^{-}_{it\omega} \quad \forall\, i \in \mathscr{I},\ t \in \mathscr{T},\ \omega \in \Omega \tag{26}$$

Constraints (27) restrict electricity flow to a commercial building

$b \in \mathscr{B}$ from an EV charging station $i \in \mathscr{I}$ at time period $t \in \mathscr{T}$ and under scenario $\omega \in \Omega$. Constraints (28) restricts the availability of V2G energy at any EV charging station $i \in \mathscr{I}$ in time period $t \in \mathscr{T}$ and under scenario $\omega \in \Omega$. This availability can be determined based on electric vehicle flow (f_{it}), percentage of discharged vehicles (β_t), and average unit power required to discharge each vehicle (γ).

$$M^{-}_{ibt\omega} \leqslant \chi^{cb}_{ibt} Y^{s-}_{ibt} \quad \forall\, i \in \mathscr{I},\ b \in \mathscr{B},\ t \in \mathscr{T},\ \omega \in \Omega \tag{27}$$

$$V_{it\omega} \leqslant \gamma \beta_t f_{it} \quad \forall\, i \in \mathscr{I},\ t \in \mathscr{T},\ \omega \in \Omega \tag{28}$$

Constraints for RES: Constraints (29) indicate that the availability of renewable energy to a charging station $i \in \mathscr{I}$ at time period $i \in \mathscr{T}$ and under scenario $\omega \in \Omega$ is restricted by the size of RES (a_i), electricity generation efficiency (η^{rr}), and the amount of solar radiation absorbed by the RES (μ_t).

$$Z^{crr}_{it\omega} \leqslant a_i \mu_t \eta^{rr} \quad \forall\, i \in \mathscr{I},\ t \in \mathscr{T},\ \omega \in \Omega \tag{29}$$

Constraints for EV Charging Station Batteries: This set of constraints (30)–(37) determine the utilized battery states for time period $t \in \mathscr{T}$ under scenario $\omega \in \Omega$. More specifically, constraints (30) indicate that each charging station $i \in \mathscr{I}$ begins with u_i number of fully-charged batteries. Constraints (31) indicate that batteries cannot be charged and discharged simultaneously in a particular time period $t \in \mathscr{T}$. Constraints (32) and (33) restrict the number of batteries that can be charged and discharged at time period $t \in \mathscr{T}$ by the availability of plug-ins (q_i^{in}/q_i^{out}) in each EV charging station $i \in \mathscr{I}$. Constraints (34) are flow balance constraints which ensure that the number of fully-charged batteries available in time $t+1$ depends on the fully-charged batteries stored in time period t along with the batteries charged, discharged, and demanded in that time period. Constraints (35) indicate that no batteries are charged at the beginning of the planning horizon. Constraints (36) restrict the number of charged batteries to the number of depleted batteries. Finally, constraints (37) restrict the number of discharged batteries and battery demanded to available fully-charged batteries.

$$W_{i,1,\omega} = u_i \quad \forall\, i \in \mathscr{I},\ \omega \in \Omega \tag{30}$$

$$Y^{c+}_{it} + Y^{c-}_{it} \leqslant 1 \quad \forall\, i \in \mathscr{I},\ t \in \mathscr{T} \tag{31}$$

$$S_{it\omega} \leqslant q_i^{in} Y^{c+}_{it} \quad \forall\, i \in \mathscr{I},\ t \in \mathscr{T},\ \omega \in \Omega \tag{32}$$

$$P_{it\omega} \leqslant q_i^{out} Y^{c-}_{it} \quad \forall\, i \in \mathscr{I},\ t \in \mathscr{T},\ \omega \in \Omega \tag{33}$$

$$W_{it\omega} - B_{it\omega} - P_{it\omega} + S_{it\omega} = W_{i,t+1,\omega} \quad \forall\, i \in \mathscr{I},\ t \in \mathscr{T} \backslash |T|,\ \omega \in \Omega \tag{34}$$

$$S_{i,1,\omega} = 0 \quad \forall\, i \in \mathscr{I},\ \omega \in \Omega \tag{35}$$

$$S_{it\omega} \leqslant u_i - W_{it\omega} \quad \forall\, i \in \mathscr{I},\ t \geqslant 2,\ t \in \mathscr{T},\ \omega \in \Omega \tag{36}$$

$$B_{it\omega} + P_{it\omega} \leqslant W_{it\omega} \quad \forall\, i \in \mathscr{I},\ t \in \mathscr{T},\ \omega \in \Omega \tag{37}$$

Constraints associated with Power Grid:

This set of constraints (38)–(46) determine the power grid states for time period $t \in \mathscr{T}$ under scenario $\omega \in \Omega$. More specifically, constraints (38) restrict the availability of grid power (g_t^{pg}) for all commercial buildings and EV charging stations while constraints (39) and (40), respectively, provide an individual grid power utilization restriction for commercial buildings (g_t^{bp}) and EV charging stations (g_t^{cp}). Constraints (41) indicate that only one-way of electricity flow is possible between power grid and a commercial building $b \in \mathscr{B}$ in time period $t \in \mathscr{T}$. Constraints (42) and (43) restrict the electricity flow among the power grid and commercial buildings $b \in \mathscr{B}$ at time period $t \in \mathscr{T}$ and under scenario $\omega \in \Omega$. Likewise, constraints (44) indicate that only one-way of electricity flow is possible between power grid and an EV charging station $i \in \mathscr{I}$ in time period $t \in \mathscr{T}$. Finally, constraints (45) and (46) restrict the electricity flow among the power grid and EV charging stations $i \in \mathscr{I}$ at time period $t \in \mathscr{T}$ and under scenario $\omega \in \Omega$.

$$\sum_{i \in \mathscr{I}} G^{+}_{it\omega} + \sum_{b \in \mathscr{B}} H^{+}_{bt\omega} \leqslant g_t^{pg} \quad \forall\, t \in \mathscr{T},\ \omega \in \Omega \tag{38}$$

$$\sum_{b \in \mathscr{B}} H^{+}_{bt\omega} \leqslant g_t^{bp} \quad \forall\, t \in \mathscr{T},\ \omega \in \Omega \tag{39}$$

$$\sum_{i \in \mathscr{I}} G^{+}_{it\omega} \leqslant g_t^{cp} \quad \forall\, t \in \mathscr{T},\ \omega \in \Omega \tag{40}$$

$$Y^{p+}_{bt} + Y^{p-}_{bt} \leqslant 1 \quad \forall\, b \in \mathscr{B},\ t \in \mathscr{T} \tag{41}$$

$$H^{+}_{bt\omega} \leqslant b^{bp}_{bt} Y^{p+}_{bt} \quad \forall\, b \in \mathscr{B},\ t \in \mathscr{T},\ \omega \in \Omega \tag{42}$$

$$H^{-}_{bt\omega} \leqslant b^{bn}_{bt} Y^{p-}_{bt} \quad \forall\, b \in \mathscr{B},\ t \in \mathscr{T},\ \omega \in \Omega \tag{43}$$

$$Y^{p+}_{it} + Y^{p-}_{it} \leqslant 1 \quad \forall\, i \in \mathscr{I},\ t \in \mathscr{T} \tag{44}$$

$$G^{+}_{it\omega} \leqslant b^{cp}_{it} Y^{p+}_{it} \quad \forall\, i \in \mathscr{I},\ t \in \mathscr{T},\ \omega \in \Omega \tag{45}$$

$$G^{-}_{it\omega} \leqslant b^{cn}_{it} Y^{p-}_{it} \quad \forall\, i \in \mathscr{I},\ t \in \mathscr{T},\ \omega \in \Omega \tag{46}$$

Binary and Non-negativity Constraints: Constraints (47) define binary restrictions for the first-stage decision variables. Likewise, constraints (48) and (49), respectively, define standard integrality and non-negativity constraints for the second-stage decision variables.

$$Z^{p}_{bt}, Z^{b}_{bt}, S^{e+}_{bt}, S^{e-}_{bt}, S^{b+}_{bt}, S^{b-}_{bt}, Y^{p+}_{bt}, Y^{p-}_{bt}, Y^{c+}_{it}, Y^{c-}_{it}, Y^{p+}_{it}, Y^{p-}_{it}, Y^{s+}_{bit}, Y^{s-}_{ibt} \in \{0, 1\} \quad \forall\, b \in \mathscr{B},\ i \in \mathscr{I},\ t \in \mathscr{T} \tag{47}$$

$$W_{it\omega}, B_{it\omega}, S_{it\omega}, P_{it\omega} \in \mathbb{Z}_{\geqslant 0} \quad \forall\, i \in \mathscr{I},\ t \in \mathscr{T},\ \omega \in \Omega \tag{48}$$

$$G^{+}_{it\omega}, G^{-}_{it\omega}, H^{+}_{bt\omega}, H^{-}_{bt\omega}, M^{+}_{bit\omega}, M^{-}_{ibt\omega}, V_{it\omega}, Z^{crr}_{it\omega}, Z^{brr}_{bt\omega}, X^{pgu}_{bt\omega}, B^{bd}_{bt\omega}, B^{b0}_{bt\omega}, X^{cb}_{bt\omega}, X^{db}_{bt\omega}, X^{pb}_{bt\omega}, X^{gb}_{bt\omega}, X^{b}_{bt\omega}, X^{ce}_{bt\omega}, X^{de}_{bt\omega}, X^{e}_{bt\omega}, U^{bd}_{bt\omega}, U^{cs}_{it\omega}, Q^{cc}_{bt\omega}, Q^{sc}_{bt\omega}, Q^{ch}_{bt\omega}, Q^{sh}_{bt\omega}, Q^{cs}_{bt\omega} \geqslant 0 \quad \forall\, i \in \mathscr{I},\ b \in \mathscr{B},\ t \in \mathscr{T},\ \omega \in \Omega \tag{49}$$

2.4. Valid inequalities

We can exploit the special structure of our problem **[BEV]** by generating a set of valid inequalities that restrict the search space of few binary variables without eliminating the optimal solution. To enhance the performance of the branch-and-bound process, the following valid inequalities are added in **[BEV]**.

- A commercial-grade battery at building $b \in \mathscr{B}$ is not capable of discharging electricity in a given time period t if no charging is made up to time period $(t-1)$.

$$\sum_{j \leqslant (t-1)} S^{e+}_{bj} \geqslant S^{e-}_{bt} \quad \forall\, b \in \mathscr{B},\ t \in \mathscr{T} \tag{50}$$

- The TES at building $b \in \mathscr{B}$ is not capable of discharging thermal energy in a given time period t if no charging is made up to time period $(t-1)$.

$$\sum_{j \leqslant (t-1)} S^{b+}_{bj} \geqslant S^{b-}_{bt} \quad \forall\, b \in \mathscr{B},\ t \in \mathscr{T} \tag{51}$$

- A battery at EV charging station $i \in \mathscr{I}$ is not capable of charging electricity in a given time period t if no discharging is made up to time period $(t-1)$.

$$\sum_{j \leqslant (t-1)} Y^{c-}_{ij} \geqslant Y^{c+}_{it} \quad \forall\, i \in \mathscr{I},\ t \in \mathscr{T} \tag{52}$$

- There is no thermal energy flow to the TES, heating, and cooling components if the PGU and/or boiler state is not switched to *on* at building $b \in \mathscr{B}$ in time period $t \in \mathscr{T}$ under scenario $\omega \in \Omega$.

$$Q^{cs}_{bt\omega} + Q^{cc}_{bt\omega} + Q^{ch}_{bt\omega} \leqslant \eta^{pgu} s^{pgu}_b Z^p_{bt} + \eta^{bo} s^{bo}_b Z^b_{bt} \quad \forall\, b \in \mathscr{B},\ t \in \mathscr{T},\ \omega \in \Omega \tag{53}$$

3. Sample average approximation algorithm

Electricity and thermal demands (e.g., heating and cooling demands) of commercial buildings, $d_{bt\omega}$, differ significantly from one hour to the next depending on different timetable of working hours, usage intensity of equipment and lighting facilities, air conditioning requirements, and many others. Likewise, the percentage of electric vehicles charged in EV charging stations, $\delta_{t\omega}$, differs significantly due to variable electric vehicle flows at EV charging stations at different time period of the day. Therefore, an extremely large number of demand scenarios need to be investigated to derive meaningful results. This not only increases the problem size for **[BEV]** but also pose serious challenge from solution standpoint. To alleviate this problem, we propose to use Sample Average Approximation (SAA) algorithm that approximates the expected second-stage operational and collaboration costs with a corresponding sample average function. The procedure is repeated with different samples until a stopping criterion (a pre-determined optimality gap) is reached. The SAA method has been successfully implemented for solving large-scale supply chain network flow related problems in [44–48]. In relation to the convergence properties and statistical performance of the SAA method, readers are referred to review the studies by Kleywegt et al. [49], Mak et al. [50], Norkin et al. [51,52].

The electricity demand for commercial buildings, $d_{bt\omega}$; $\forall\, b \in \mathscr{B}, t \in \mathscr{T}, \omega \in \Omega$, and the percentage of electric vehicles charged in a charging station $i \in \mathscr{I}$ at time period t, $\delta_{t\omega}$; $\forall\, t \in \mathscr{T}, \omega \in \Omega$ are assumed to follow a normal distribution. The SAA method generates N samples ($|N| < |\Omega|$) and approximates the objective function value of the second-stage problem as follows:

$$\mathbb{E}[Q(\mathbf{Z}, \omega)] := \frac{1}{|N|}\sum_{n\in N} Q(\mathbf{Z}, \omega^n)$$

where $Q(\mathbf{Z}, \omega^n)$ is a solution of the second-stage problem for a given value of $\mathbf{Z}$ under scenario ω^n. Problem [**BEV**] is now approximated by the following SAA problem:

$$\textit{Minimize}\ \left\{ Z^m_N = \sum_{t\in\mathscr{T}}\sum_{b\in\mathscr{B}} (\psi^{pgu}_b Z^p_{bt} + \psi^{bo}_b Z^b_{bt}) + \frac{1}{|N|}\sum_{n\in N} Q(\mathbf{Z}, \omega^n) \right\}$$

As the sample size increases, the optimal solution approximated by the above equation converges with probability one to an optimal solution of the original problem [**BEV**] [49]. By solving the SAA problem within an absolute optimality gap $\delta \geqslant 0$, the sample size $|N|$ is estimated to guarantee an ϵ-optimal solution to the true problem with probability at least equal to $(1-\alpha)$ as follows:

$$|N| \geqslant \frac{3\sigma^2_{max}}{(\epsilon-\delta)^2}(|\mathscr{B}||\mathscr{T}|(log 2) - log\alpha)$$

where $\epsilon > \delta$, $\alpha \in (0, 1)$, and σ^2_{max} is a maximal variance of certain function differences [49]. It is worth noting that choosing sample size $|N|$ is a trade-off between the solution quality and required computational time. Note that the above formula may provide a conservative sample size estimation for practical applications [49]. In each iteration of the SAA method, valid statistical lower and upper bounds are provided for the original problem [**BEV**] and the process terminates when the gap between the bounds falls below a pre-determined threshold value. The following steps briefly summarize the SAA method to solve problem [**BEV**].

Step 1: Generate set M of independent commercial building load and percentage of electric vehicles charged in an EV charging station scenarios, each of size $|N|$, i.e., $\{d_{bt\omega^1_m}, d_{bt\omega^2_m}, ..., d_{bt\omega^{|N|}_m}\}$, $\forall\, m \in M, b \in \mathscr{B}, t \in \mathscr{T}$ and $\{\delta_{t\omega^1_m}, \delta_{t\omega^2_m}, ..., \delta_{t\omega^{|N|}_m}\}$, $\forall\, m \in M, t \in \mathscr{T}$, respectively. Then, solve the corresponding SAA for each generated sample consisting of $|N|$ realizations of independently and identically distributed ($i.\ i.\ d.$) random scenarios. The optimal objective function value and the optimal solution are denoted by Z^m_N and $\hat{Z}_M$, respectively.

$$Z^m_N = \sum_{b\in\mathscr{B}}\sum_{t\in\mathscr{T}} (\psi^{pgu}_b Z^p_{bt} + \psi^{bo}_b Z^b_{bt}) + \frac{1}{|N|}\sum_{n\in N} Q(\mathbf{Z}, \omega^n)$$

Step 2: Compute the *average* of all optimal objective function values obtained from the SAA problems, $\overline{Z}^M_N$, as follows:

$$\overline{Z}^M_N = \frac{1}{|M|}\sum_{m\in M} Z^m_N$$

where, $\overline{Z}^M_N$ provides a statistical lower bound on the optimal objective function value for the original problem **[BEV]** [52]. Since $Z^1_N, Z^2_N, ..., Z^M_N$ generated samples are independent, the corresponding variance of $\overline{Z}^M_N$, i.e., $\sigma^2_{\overline{Z}^M_N}$, is given by:

$$\sigma^2_{\overline{Z}^M_N} = \frac{1}{(|M|-1)(|M|)}\sum_{m\in M} (Z^M_N - \overline{Z}^M_N)^2$$

Step 3: Generate set N' i.e., a large sample size where $|N'| \gg |N|$ to compute the estimated optimal objective solution of the SAA method [49]. This estimator, which is the upper bound of the optimal solution on the generated sample size $|N'|$, is obtained by one of the solutions of $\hat{Z}_M$ as follows:

$$Z_{N'}(\hat{Z}_M) = \sum_{b\in\mathscr{B}}\sum_{t\in\mathscr{T}} (\psi^{pgu}_b Z^p_{bt} + \psi^{bo}_b Z^b_{bt}) + \frac{1}{|N'|}\sum_{n\in N'} Q(\mathbf{Z}, \omega^n)$$

In each iteration, the estimator upper bound $Z_{N'}(\hat{Z}_M)$ is updated. The variance of this estimator upper bound is calculated as follows:

$$\sigma^2_{N'}(\hat{Z}_M) = \frac{1}{(|N'-1|)(|N'|)} \sum_{n\in N'} \left\{ \sum_{b\in\mathscr{B}}\sum_{t\in\mathscr{T}} (\psi^{pgu}_b Z^p_{bt} + \psi^{bo}_b Z^b_{bt}) + Q(\hat{Z}_M, \omega^n) - Z_{N'}(\hat{Z}_M) \right\}^2$$

Step 4: Compute the SAA gap, $Gap_{(N,N')}$, and the variance of this gap, $\sigma^2_{Gap_{(N,N')}}$, using the estimators determined in **Steps 2** and **3**.

$$Gap_{(N,N')}(\widetilde{Z}) = Z_{N'}(\hat{Z}_M) -- \overline{Z}^M_N$$

$$\sigma^2_{Gap_{(N,N')}} = \sigma^2_{N'}(\hat{Z}_M) + \sigma^2_{\overline{Z}^M_N}$$

The confidence interval for the optimality gap is then calculated as follows:

$$Z_{N'}(\hat{Z}_M) - \overline{Z}^M_N + z_\alpha\{\sigma^2_{N'}(\hat{Z}_M) + \sigma^2_{\overline{Z}^M_N}\}^{1/2}$$

with $z_\alpha := \Phi^{-1}(1-\alpha)$, where $\Phi(z)$ is the cumulative distribution function of the standard normal distribution.

Step 5: Define the best solution among the solutions of $\hat{Z}_M(\,\forall\, m \in M)$ that represents the lowest upper bound $Z_{N'}(\hat{Z}_M)$.

4. Computational study and managerial insights

This section utilizes SAA method to solve model **[BEV]** and to draw managerial insights from a real life case study. We use the city of San

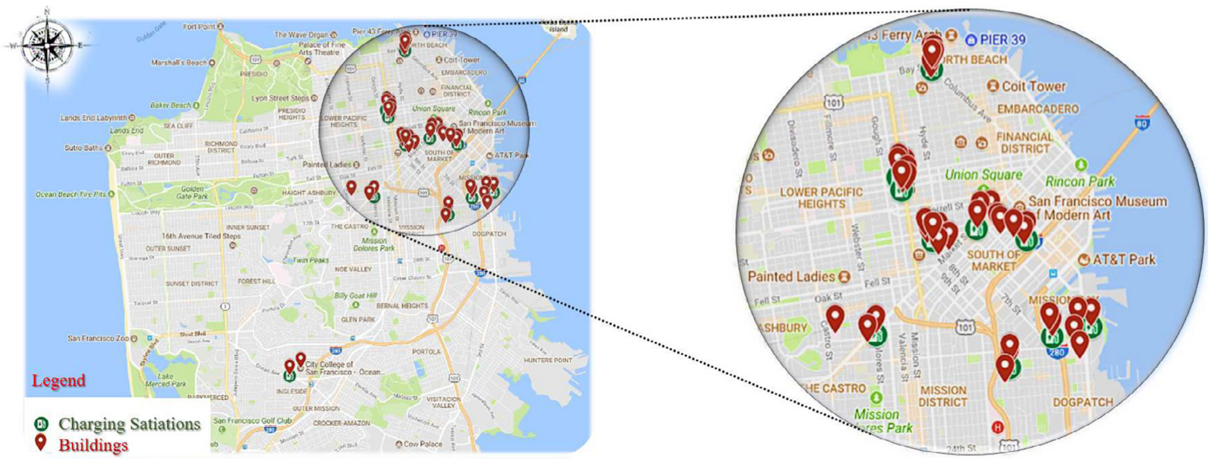

Fig. 3. EV charging station distribution with nearby commercial buildings in San Francisco.

Francisco as a testbed to visualize and validate the modeling results. The proposed mathematical model and the solution algorithm are coded in GAMS 24.2.1 [53] on a desktop computer equipped with an Intel Core i7 3.50 GHz processor and 32 GB RAM. The optimization solver used is ILOG CPLEX 12.6.[2] All costs are calculated based on 2018 dollars value. The following subsections describe the input parameters used in this study, present the computational performance of solving model **[BEV]** using the SAA algorithm, and to the end draw managerial insights from a real life case study.

4.1. Data description

Since San Francisco has a strong-growing EV population, it was chosen as a testing ground to visualize and validate the modeling results. In addition, it has a reputation as being one of the nation's most environmentally conscious cities. Several factors contribute to this status, not the least of which San Francisco also recognizes as one of the wealthiest cities in the country. Furthermore, San Francisco offers some of the most electric vehicle-friendly incentives for EV owners at both the state and local levels. For example, under the *Bay Area Air Quality Management District's EV Rebate Program*, public agencies can receive an additional \$2500 and \$1000 for the purchase of an EV and plug-in hybrid EV, respectively [54]. Surplus electricity from one or more commercial buildings $b \in \mathscr{B}_i$ may be able to share with a nearby EV charging station(s) $i \in \mathscr{I}_b$ and vice versa. This being the case, 11 fast EV charging stations ($|\mathscr{I}| = 11$) and 43 commercial buildings ($|\mathscr{B}| = 43$), located near those charging stations, are selected from San Francisco to construct a real life case study [55]. Fig. 3 demonstrates the distribution of fast EV charging station locations along with their nearby commercial buildings.

The availability of electricity obtained from a solar panel during a typical day in San Francisco is obtained from a study by [56]. We set the size of solar panels 100 m^2 and 75 m^2 for commercial buildings (a_b) and EV charging stations (a_i), respectively. Commercial and industrial time-of-use (TOU) rates are adopted from [57] to determine unit electricity transaction prices for c_t^+, c_t^-, and c_t^t. Based on the TOU rate, 1:00 P.M. through 8:00 P.M. are the *peak* hours of electricity usage when the electricity transaction price is high. On the other hand, 5:00 A.M. through 12:00 P.M. along with 9:00 P.M. through 11:00 P.M. are the *sub-peak* hours of electricity usage when the electricity transaction price is lower compared to peak hours. All other hours throughout a day are *off-peak* hours with the lowest price. Fig. 4 represents different electricity usage hours. The hourly electricity pricing plan for V2G (c_t^{v2g}) is obtained from [58].

The values of $d_{bt\omega}$ are estimated from the TOU rate, while f_{it} is determined based on the number of EVs available at San Francisco in 2016 [59]. Other factors such as population density along with the number of hospitals and colleges located near major roads are considered to project f_{it}. We set $\delta_{t\omega}$ and β_t to be 40% and 5%, respectively, for the base case scenario. The average unit power charging requirement λ and power discharged from each car γ are set to be 25.7 kWh, respectively. The daily fuel consumption capacity of the PGU (s_b^{pgu}) is set to be 200 *gallon*. The grid power availability for each commercial building (b_{bt}^{bp}) and EV charging station (b_{it}^{cp}) are set to be 200 kWh and 250 kWh, respectively. The commercial-grade battery capacity (s_b^{bs}) is set to be 100 kW. For simplification purposes, the minimum and maximum percentages of SoC/charging capacity/discharging capacity of a commercial-grade battery/TES are set to be 20% and 90%, respectively, while their charging and discharging efficiencies (η) are both set to be 90%. Unit penalty cost of power shortage (c_t^{us}) is determined based on the following formula: $c_t^{us} > max\{c_t^+, c_t^t, c^f\}$. Finally, the unit battery storage cost in an EV charging station (c_t^s) is set to be 0.02 \$/h.

A study, performed by Gamou et al. [60], proposes an optimal unit sizing method for co-generation. It reveals that energy demand roughly follows a normal probability distribution in which 95% of the whole area is within the range of ±20% of the average energy demands. This being the case, the energy demand of each commercial building $b \in \mathscr{B}$ follows a multivariate normal distribution $\mathscr{N}(\boldsymbol{\mu}_1, \boldsymbol{\Sigma}_1)$ in each time period $t \in \mathscr{T}$, where vector $\boldsymbol{\mu}_1$ and matrix $\boldsymbol{\Sigma}_1$ define the projected demand and forecasting error, respectively. Based on this commercial building demand distribution, Monte Carlo simulation is employed to generate scenarios for $d_{bt\omega}$.

Uncertainty exists in the percentage of EVs that require charging in a given time period $t \in \mathscr{T}$. This percentage varies significantly from hour to hour due to various reasons such as remaining *state of charge* (SoC[3]) of EV batteries, car owner's willingness to stay at an EV charging station, and the timing for charging and discharging EV cars (e.g., peak, sub-peak, and off-peak hours). Therefore, a large set of scenarios are required to accurately estimate $\delta_{t\omega}$. Likewise, Monte Carlo simulation is implemented to generate scenarios for $\delta_{t\omega}$. The generated samples are independent and identically distributed (*iid*) random variables. Therefore, $\delta_{t\omega}$ follows a multivariate normal distribution $\mathscr{N}(\boldsymbol{\mu}_2, \boldsymbol{\Sigma}_2)$ in each time period $t \in \mathscr{T}$, where vectors $\boldsymbol{\mu}_2$ and $\boldsymbol{\Sigma}_2$ are defined as the forecasted EV charging percentage and forecasting error, respectively. It is worth noting that the error terms are also considered to be independent and normally distributed with mean zero and variance σ^2. The Monte

[2] Available from: https://www.ibm.com/products/ilog-cplex-optimization-studio.

[3] SoC is the ratio of available energy to the maximum storage energy in electric vehicle battery.

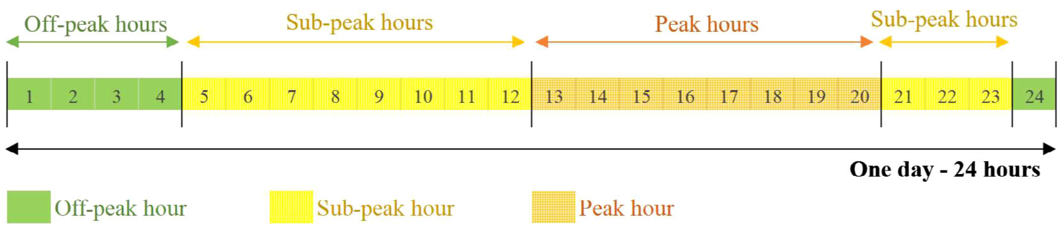

Fig. 4. Electricity usage hours.

Table 1
Deterministic equivalent problem size for model **[BEV]**.

Sizes	Instances	$\lvert\mathscr{I}\rvert$	$\lvert\mathscr{B}\rvert$	$\lvert\mathscr{T}\rvert$	Variables				Total constraints
					Binary	Integer	Continuous	Total	
Small	1	2	8	12	480	96	2520	3096	5754
	2	2	8	24	960	192	5040	6192	11,526
	3	3	12	12	720	144	4068	4932	8901
	4	3	12	24	1440	288	8136	9864	17,829
	5	4	16	12	960	192	5808	6960	12,240
	6	4	16	24	1920	384	11,616	13,920	24,516
	7	5	20	12	1200	240	7740	9180	15,771
	8	5	20	24	2400	480	15,480	18,360	31,587
	9	6	24	12	1440	288	9864	11,592	19,494
	10	6	24	24	2880	576	19,728	23,184	39,042
Medium	1	8	32	24	3840	768	29,376	33,984	55,104
	2	8	32	72	11,520	2304	88,128	101,952	165,456
	3	9	36	24	4320	864	34,776	39,960	63,711
	4	9	36	72	12,960	2592	104,328	119,880	191,295
	5	10	40	24	4800	960	40,560	46,320	72,702
	6	10	40	72	14,400	2880	121,680	138,960	218,286
	7	11	43	24	5160	1056	45,696	51,912	80,351
	8	11	43	72	15,480	3168	137,088	155,736	241,247
	9	12	48	24	5760	1152	53,280	60,192	91,836
	10	12	48	72	17,280	3456	159,840	180,576	275,724
Large	1	15	60	168	50,400	10,080	526,680	587,160	864,729
	2	15	60	360	108,000	21,600	1,128,600	1,258,200	1,853,145
	3	17	68	168	57,120	11,424	642,600	711,144	1,025,655
	4	17	68	360	122,400	24,480	1,377,000	1,523,880	2,198,007
	5	20	80	168	67,200	13,440	836,640	917,280	1,287,204
	6	20	80	360	144,000	28,800	1,792,800	1,965,600	2,758,500
	7	22	88	168	73,920	14,784	979,440	1,068,144	1,475,010
	8	22	88	360	158,400	31,680	2,098,800	2,288,880	3,160,962
	9	25	100	168	84,000	16,800	1,213,800	1,314,600	1,776,879
	10	25	100	360	180,000	36,000	2,601,000	2,817,000	3,807,855

Carlo simulation generates a large number of scenarios with equal probabilities $1/|N|$, where N is a set of sample scenarios.

4.2. Computational performance of the SAA algorithm

The subsection presents how the valid inequalities and SAA method, proposed in Sections 2.4 and 3, impact the computational performance of model **[BEV]**. To help the readers follow our approaches, we have used the following notations to represent the algorithms:

- **[CPLEX]**: Model **[BEV]** is solved by CPLEX
- **[CPLEX-VI]**: Model **[BEV]** is solved by CPLEX + valid inequalities (VI)
- **[SAA]**: The SAA method
- **[SAA-VI]**: The SAA method + valid inequalities (VI)

Table 1 presents the deterministic equivalent problem size for model **[BEV]**. We vary the number of charging stations $|\mathscr{I}|$, commercial buildings $|\mathscr{B}|$, and time period $|\mathscr{T}|$ to obtain 30 different problem instances. These problem instances are broadly classified into three different sizes: *small*, *medium*, and *large*. The maximum size for the *small* problem instance is set up to 6 charging stations, 24 commercial buildings, and 24 h i.e., $|\mathscr{I}| = 6$, $|\mathscr{B}| = 24$, and $|\mathscr{T}| = 24$. Likewise, a maximum of 12 charging stations, 48 commercial buildings, and 72 h (3 days) i.e., $|\mathscr{I}| = 12$, $|\mathscr{B}| = 48$, and $|\mathscr{T}| = 72$ are considered for *medium* problem instance, and 25 charging stations, 100 commercial buildings, and 360 h (15 days) i.e., $|\mathscr{I}| = 25$, $|\mathscr{B}| = 100$, and $|\mathscr{T}| = 360$ are considered for *large* problem instance to solve model **[BEV]**, respectively.

Table 2 presents the computational performances from **[CPLEX]**, **[CPLEX-VI]**, **[SAA]**, and **[SAA-VI]** under three different test sizes as reported in Table 1. The performance of each approaches are represented by *percentage deviation (gap)* Δf_i (in %) and *running time* T (in *seconds*). The gap between the upper and lower bound of the i^{th} solution approach, denoted by UB_i and LB_i, respectively, is used to calculate Δf_i i.e., $\Delta f_i(\%) = \left(\frac{UB_i - LB_{Best}}{LB_{Best}}\right) \times 100\%$; $\forall\, i \in \mathscr{S}$, where $\mathscr{S} = \{[\textbf{CPLEX}], [\textbf{CPLEX–VI}], [\textbf{SAA}], [\textbf{SAA–VI}]\}$ and $LB_{Best} = Max\{LB_i\}$; $\forall\, i \in \mathscr{S}$. All solution approaches are terminated when at least one of the following criteria is satisfied: (a) the gap falls below a threshold value ε, i.e., $\Delta f_i(\%) \leqslant \varepsilon$ or (b) the maximum running time limit, CT^{max}, is reached. In this study, the stopping criteria are set as $\varepsilon = 1.0\%$ and $CT^{max} = 3600$ s. Additionally, we set $N = 20$ and

Table 2
Result comparison from **[CPLEX]**, **[CPLEX-VI]**, **[SAA]**, and **[SAA-VI]**.

Size	Case	[CPLEX]		[CPLEX-VI]		[SAA]		[SAA-VI]	
		Δf (%)	T (s)	Δf (%)	T (s)	Δf (%)	T (s)	Δf (%)	T (s)
Small	1	0.09	**6.63**	0.16	7.04	0.08	8.61	0.11	8.91
	2	0.13	**11.24**	0.17	13.47	0.14	15.66	0.19	13.87
	3	0.14	9.57	0.15	**8.25**	0.23	11.47	0.34	12.62
	4	0.23	19.79	0.33	**12.98**	0.29	22.64	0.27	20.74
	5	0.16	**11.78**	0..64	14.82	0.18	16.85	0.42	14.97
	6	0.28	27.02	0.49	**19.88**	0.44	32.87	0.16	29.14
	7	0.34	17.64	0.67	**10.24**	0.36	19.64	0.27	18.35
	8	0.46	38.06	0.34	**24.38**	0.28	42.05	0.25	33.64
	9	0.35	22.09	0.75	**15.09**	0.74	25.67	0.55	23.78
	10	0.24	49.87	0.41	38.54	0.68	**30.41**	0.28	35.64
Average		0.24	21.37	0.39	**16.47**	0.34	22.59	0.28	21.17
Medium	1	0.51	865.06	0.38	425.08	0.25	**171.73**	0.77	188.69
	2	12.95	CT^{max}	7.63	CT^{max}	0.76	1336.87	0.39	**589.67**
	3	0.85	2912.59	0.73	3152.67	0.37	1187.63	0.14	**468.97**
	4	14.25	CT^{max}	9.49	CT^{max}	0.84	1763.87	0.64	**785.41**
	5	7.12	CT^{max}	4.97	CT^{max}	0.53	1587.09	0.26	**597.28**
	6	15.63	CT^{max}	10.23	CT^{max}	0.84	2364.43	0.72	**987.68**
	7	8.02	CT^{max}	5.34	CT^{max}	0.65	1873.04	0.38	**653.41**
	8	16.52	CT^{max}	11.41	CT^{max}	0.84	3174.58	0.12	**1009.34**
	9	9.12	CT^{max}	6.58	CT^{max}	0.58	2141.78	0.62	**763.14**
	10	18.71	CT^{max}	12.54	CT^{max}	0.46	3374.21	0.44	**1143.81**
Average		10.37	3257.77	6.93	3237.78	0.61	1897.52	0.45	**718.74**
Large	1	22.88	CT^{max}	17.54	CT^{max}	1.89	CT^{max}	0.63	**1244.35**
	2	*OM*	–	*OM*	–	2.24	CT^{max}	0.41	**1465.38**
	3	*OM*	–	*OM*	–	3.14	CT^{max}	0.83	**1301.41**
	4	*OM*	–	*OM*	–	5.73	CT^{max}	0.67	**2354.25**
	5	*OM*	–	*OM*	–	2.12	CT^{max}	0.29	**1423.12**
	6	*OM*	–	*OM*	–	8.67	CT^{max}	**1.09**	CT^{max}
	7	*OM*	–	*OM*	–	3.54	CT^{max}	0.38	**1478.63**
	8	*OM*	–	*OM*	–	15.96	CT^{max}	**1.27**	CT^{max}
	9	*OM*	–	*OM*	–	4.63	CT^{max}	0.89	**1396.54**
	10	*OM*	–	*OM*	–	18.54	CT^{max}	**1.64**	CT^{max}
Average		22.88	CT^{max}	17.54	CT^{max}	6.65	CT^{max}	0.81	**2146.37**
Total average		6.14	1732.92	4.52	1721.07	2.53	1840.04	0.51	**962.09**

CT^{max}: maximum time limit.
OM: out of memory.

$N' = 1000$ to evaluate the performance of the **[SAA]** algorithm. In reporting the computational performance of the approaches, we highlight the approach which is solved in less than the stopping criteria ϵ while simultaneously producing the smallest running time (represented by $T(s)$ in Table 2) for a given test instance. Otherwise, if such a quality solution is not found within the maximum time limit, then the algorithm with the smallest optimality gap (represented by $\Delta f(\%)$ in Table 2) is highlighted. In the following, we summarize our observations for Table 2.

- **[CPLEX-VI]** demonstrates high quality in solving **[BEV]** for *small* scale problem instances. However, both **[CPLEX]** and **[CPLEX-VI]** are unable to produce satisfactory optimality gaps to solve *medium* scale problem instances within the prespecified time limit CT^{max}. On average, we observe a 10.37% and 6.93% optimality gap for **[CPLEX]** and **[CPLEX-VI]**, respectively, while 8/10 medium scale problem instances remain unsolved within the time limit. For *large* scale problem instances, both **[CPLEX]** and **[CPLEX-VI]** gets *out of memory* in 9/10 instances indicating their inability to solve model **[BEV]** in large scale problem settings.
- **[SAA-VI]** appears to be the best option to solve model **[BEV]** for *medium* and *large* scale problem instances. For medium scale problem instances, on average **[SAA-VI]** saves 62.15% time over **[SAA]** while producing 0.45% optimality gap within the time limit. For large scale problem instances, when both **[CPLEX]** and **[CPLEX-VI]** gets *out of memory* and **[SAA]** is unable to solve any problem instances within the time limit, **[SAA-VI]** solves 7/10 instances within the time limit and the remaining 3 instances within a reasonable optimality gap.

To summarize, **[SAA-VI]** seems to offer high quality solutions consistently over its counterparts in solving model **[BEV]** within the experimental range.

4.3. Experimental results

4.3.1. Base case results

The first set of experiments report the base case results obtained from solving model **[BEV]** using the real life case study developed for San Francisco. Fig. 5(a) and (b) show the average utilization of the various power sources (e.g., power grid (PG), PGU, RES, battery, and energy collaboration between commercial buildings to charging stations (CS) and vice versa) to satisfy electricity demand for a commercial building and an EV charging station under the base case scenario. Further, Fig. 5(c) shows the average number of batteries swapped ($B_{it\omega}$), charged ($W_{it\omega}$), charging ($S_{it\omega}$), and discharging ($P_{it\omega}$) at a given charging

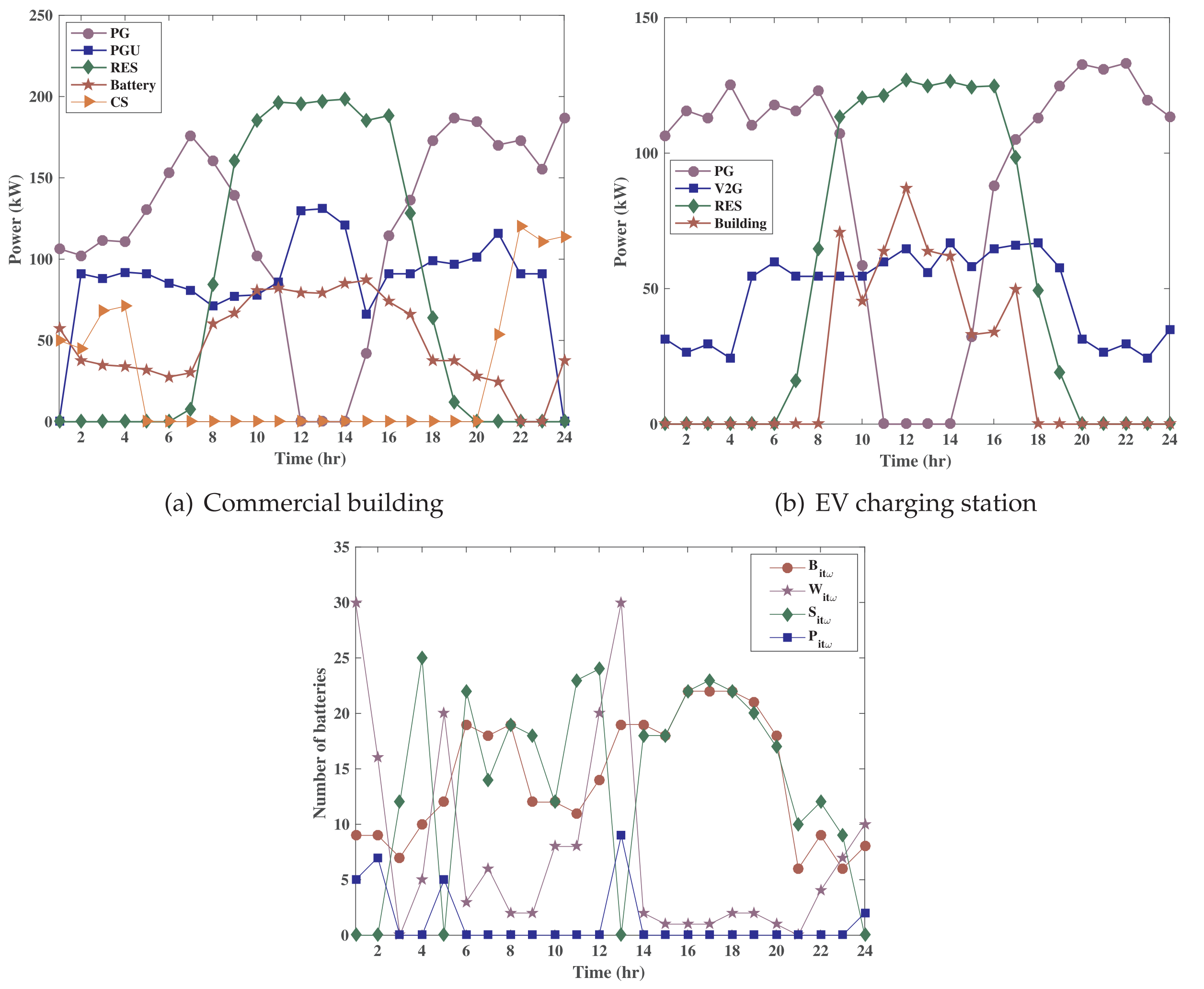

(a) Commercial building

(b) EV charging station

(c) Swapping batteries at EV charging station

Fig. 5. Average resource power utilization in a typical day for a building and a charging station under the base case scenario.

station $i \in \mathscr{I}$ in different time period $t \in \mathscr{T}$ of a day.

Results in Fig. 5(a) and (b) clearly indicate that the electricity demands for commercial buildings and EV charging stations are primarily satisfied via power grid (PG) during the time period from 5:00 P.M. to 8:00 A.M. (almost at the end of peak hours, whole off-peak hours, and at the beginning of the first sub-peak hours). Note that the electricity purchasing price from the power grid (c_t^+) is minimum during this time period of the day. Additionally, it is observed that the electricity flow from power grid to commercial buildings ($G_{it\omega}^+$) and EV charging stations ($H_{it\omega}^+$) reaches it's minimum during 11:00 A.M. to 2:00 P.M. i.e., $G_{it\omega}^+ = H_{it\omega}^+ \simeq 0$, primarily, due to high c_t^+ price and the peak availability of RES during that time period of the day. It is worth noting that commercial buildings share electricity with EV charging stations during the off-peak hours while the reverse occurring during the peak hours. Finally, Fig. 5(c) shows that majority of the battery swapping $B_{it\omega}$ and charging operations $S_{it\omega}$ are performed during the day time period to satisfy the peak energy demand for the charging stations.

4.3.2. *Impact of power transaction restriction (χ_{bit}^{bc} and χ_{ibt}^{cb}) on system performance*

This set of experiments study the impact of *power transaction* restrictions between related commercial buildings and EV charging stations and vice versa i.e., χ_{bit}^{bc} and χ_{ibt}^{cb}, on overall energy network cost. We set the base case values for χ_{bit}^{bc} and χ_{ibt}^{cb} to 100 kWh. We then vary this value to ±10% and ±20% and observe their impact on overall energy network cost. Table 3 shows the operation costs of commercial buildings, EV charging stations, and overall network costs based on changes in the power transaction limits. Results in Table 3 indicate that if the values of χ_{bit}^{bc} and χ_{ibt}^{cb} are relaxed, then significant cost savings can be achieved from the proposed collaborative system. For instance, if the values of χ_{bit}^{bc} and χ_{ibt}^{cb} are relaxed by 20%, we then observe an additional 6.72% cost savings from the proposed collaborative system. We construct another scenario where it is assumed that *no energy collaboration* is permitted between the commercial buildings and EV charging

Table 3
System performance under changes in χ_{bit}^{bc} and χ_{ibt}^{cb}.

% change in $\chi_{bit}^{bc}/\chi_{ibt}^{cb}$	Cost ($)			Cost savings (%)
	Buildings	Charging stations	Overall network	
−20%	15,813	1095	16,908	−6.88
−10%	15,326	1023	16,349	−3.35
0% (Base case)	14,878	941	15,820	0.00
10%	14,464	873	15,338	3.04
20%	13,941	816	14,757	6.72
No power transaction	16,896	1,176	18,073	−14.24

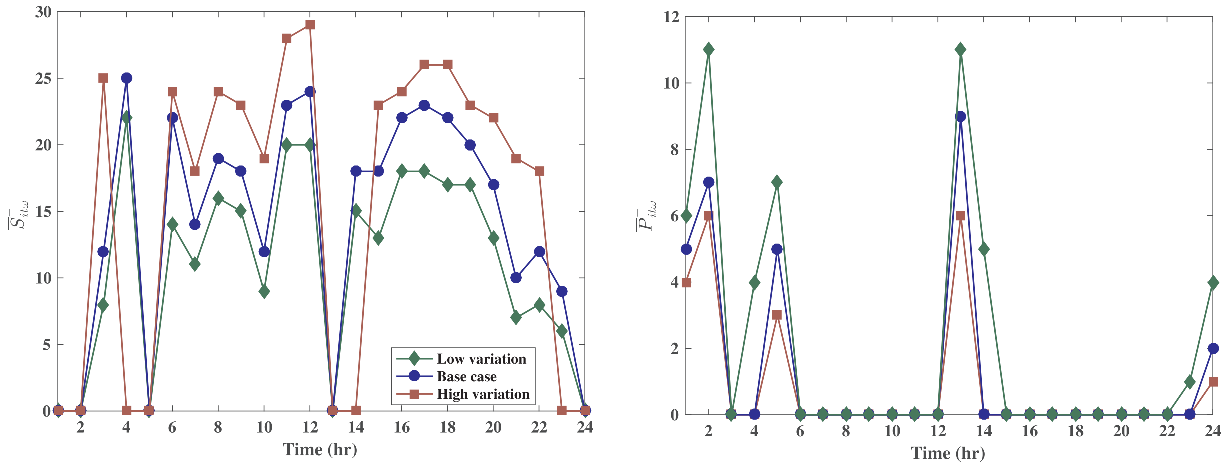

(a) Charged EV batteries vs. time

(b) Discharged EV batteries vs. time

Fig. 6. Impact of charging station demand variability on charged and discharged EV batteries.

stations i.e., $\chi_{bit}^{bc} = \chi_{ibt}^{cb} = 0\,;\forall\, b \in \mathscr{B},\ i \in \mathscr{I},\ t \in \mathscr{T}$. Results show that a 14.24% increase in energy cost which could have been saved if collaboration exists between the commercial buildings and EV charging stations. In overall, we observe that the power transaction limits (χ_{bit}^{bc} and χ_{ibt}^{cb}) have a considerable effect on the overall energy network cost.

4.3.3. Impact of demand variability on system performance

This set of experiments examine the impact of *demand variability* on overall system performance. Let $\overline{d}_{bt}$ and σ_{bt}^2 be the *mean* and *variance* of demand related to commercial buildings $b \in \mathscr{B}$ at time period $t \in \mathscr{T}$, respectively. Likewise, we define $\overline{\delta}_t$ and σ_t^2 to be the *mean* and *variance* of the percentage of electric vehicles charged at time period $t \in \mathscr{T}$, respectively. We set three different demand variation levels: *low* ($\sigma_{bt}^2 = 5\%\overline{d}_{bt}$ and $\sigma_t^2 = 5\%\overline{\delta}_t$), *medium* ($\sigma_{bt}^2 = 15\%\overline{d}_{bt}$ and $\sigma_t^2 = 15\%\overline{\delta}_t$ – set as base case), and *high* ($\sigma_{bt}^2 = 50\%\overline{d}_{bt}$ and $\sigma_t^2 = 50\%\overline{\delta}_t$). We then implement Monte Carlo simulation techniques to generate scenarios for those different variation levels.

Demand variability significantly impacts the electricity and thermal energy management for a building. Demand fluctuations in electricity and thermal energy are usually controlled via a commercial grade battery system and the TES where a high level of demand variation leads to more energy storage in the commercial-grade battery and TES while less electricity flow to the power grid and associated EV charging stations. Similarly, low demand variation levels lead to less storage in the buffers and more electricity flow to the power grid and associated EV charging stations. Likewise, decisions about the number of charged, discharged, and exchanged batteries and, consequently, the number of stored batteries at the EV charging stations changes significantly depending upon the variation in the percentage of EVs that need to be charged in a give time period. Thus, a high level of demand variation may lead to less electricity flow to the power grid and related commercial buildings while higher number of batteries stored at any EV charging stations and vice versa. This is reflected in Figs. 6 and 7 where it can be seen that how decisions such as *average* number of batteries charged ($\overline{S}_{it\omega}$) and discharged ($\overline{P}_{it\omega}$) at EV charging stations and electricity flow from commercial buildings ($\overline{H}_{bt\omega}^{-}$) and EV charging stations ($\overline{G}_{it\omega}^{-}$) to power grid are impacted by different demand fluctuation levels. Experimental results clearly indicate that $\overline{S}_{it\omega}$, $\overline{P}_{it\omega}$, $\overline{H}_{bt\omega}^{-}$, and $\overline{G}_{it\omega}^{-}$ decisions are highly impacted by different demand variation levels. It is observed that high level of demand fluctuations mandate more batteries to charge ($\overline{S}_{it\omega}$) in a given charging station (shown in Fig. 6(a)). This indirectly results less electricity flow from EV charging stations to power grid ($\overline{G}_{it\omega}^{-}$) and vice versa (shown in Fig. 7(b)). Finally, we observe that majority of the electricity flow from commercial buildings and charging stations to power grid occurs during 10:0 A.M. till 3:0 P.M. This may be due to the fact that both the availabilities of renewable energy resources and V2G power become peak during that time period of the day which can support the energy demands for the

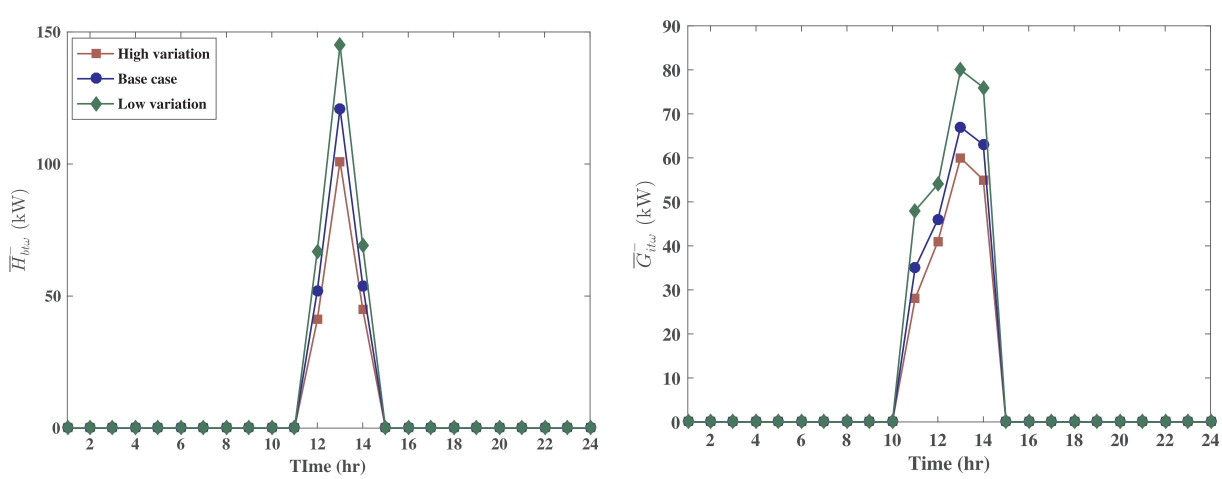

(a) Commercial building to power grid

(b) EV charging station to power grid

Fig. 7. Impact of buildings and charging stations demand variability on electricity flow to the power grid.

Table 4
Description of the grid power unavailability scenarios.

Scenario	Explanation
1	Grid power unavailable between 1:0 and 4:0 A.M.
2	Grid power unavailable between 5:0 and 8:0 A.M.
3	Grid power unavailable between 9:0 A.M. and 12:0 P.M.
4	Grid power unavailable between 1:0 and 4:0 P.M.
5	Grid power unavailable between 5:0 and 8:0 P.M.
6	Grid power unavailable between 9:0 P.M. and 12:0 A.M.

commercial buildings and EV charging stations.

4.3.4. Impact of power grid disruption on system performance

Transmission line failure might occur due to excessive power flow between the power grid (PG) and a commercial building or EV charging station, or by a man-made/natural disaster. Since the failure of power grid connection has an important effect on the utilization of different other power resources, we perform sensitivity analysis on its impact of the overall system performance. A commercial building or an EV charging station is selected randomly and its connection with the power grid is terminated for several consecutive time periods. Table 4 describes the different grid power unavailability scenarios constructed to run the case experiments. The experimental results under these scenarios are then presented in Table 5. Table 5 reports the percentage changes in utilized resources (from the base case results as discussed in Section 4.3.1) at a commercial building and an EV charging station under different power grid disruption scenarios.

Results in Table 5 clearly indicate that the utilization of different power resources (e.g., PGU, RES, V2G, battery) are significantly impacted by the time when the grid power becomes unavailable. For instance, if the grid power becomes unavailable between 5:0 and 8:0 P.M. (scenario 5) of a regular day, the overall utilization of grid power drops by 24.89% and 21.23% from the base case scenario for commercial buildings and EV charging stations, respectively. It can be observed that to offset this power unavailability, PGU and battery for commercial buildings and V2G and buildings for EV charging stations are primarily used. It can also be noted that upon disruption, charging stations rely more on commercial buildings than vice versa. For instance, depending on the type of scenario, the increment of energy sharing from charging station to commercial buildings (denoted by column heading *CS* (%) in Table 5) lies in between (2.68–3.87)%. On the other hand, the number varies between (4.37–8.91)% for the EV charging stations under the same experimental conditions. Finally, it can be noted that we observe no significant changes in RES utilization from the base case scenario even after the grid power becomes unavailable under different scenarios. This may be due to the fact that the RES is already utilized almost on its maximum capacity under the base case scenario.

4.3.5. Impact of changes in RES size (a_b/a_i) on system cost

The last of experiments study the impact of changes in RES sizes (a_b/a_i) on overall system cost. The sizes of RES play an important role on the utilization of other energy sources (e.g., grid, V2G), particularly during the first sub-peak hours and peak hours on a regular day. Therefore, sensitivity analyses are conducted (shown in Table 6) to examine the impact of changes in a_b and a_i sizes on overall system cost with and without the collaboration between the commercial buildings and EV charging stations. To run these experiments, we vary the sizes of a_b and a_i by ±25% and ±50% from the base case settings. Results in Table 6 clearly indicate that significant cost savings can be achieved (shown in the last column of Table 6) with an increase in a_b and a_i sizes and for the case when collaboration exists between the commercial buildings and EV charging stations. For instance, approximately 23.7% cost savings can be achieved if energy collaboration exists between the commercial buildings and EV charging stations and when a_b and a_i sizes are increased by 50% from the base case sizes. To summarize, we observe that the overall system cost is highly sensitive to the changes in a_b and a_i sizes and the existence of collaboration between the commercial buildings and EV charging stations.

Table 6
Impact of changes in RES size on system cost.

Change in a_b/a_i (%)	Operating cost ($)						Cost savings (%)
	With collaboration			Without collaboration			
	Building	CS	Total	Building	CS	Total	
−50%	16,954	1215	18,170	17,865	1347	19,213	5.7
−25%	15,581	1135	16,717	17,123	1203	18,327	9.6
0% (Base case)	14,878	941	15,820	16,896	1176	18,073	14.2
25%	14,123	836	14,960	16,763	1104	17,868	19.4
50%	13,563	781	14,344	16,684	1062	17,747	23.7

5. Conclusion

This study proposes a novel two-way collaborative energy sharing optimization framework between power grid and multiple commercial buildings and EV charging stations. A two-stage stochastic mixed-integer linear programming model **[BEV]** is formulated to determine the key operational factors with an aim of minimizing the overall system cost under power demand uncertainty. The key operational decisions for commercial buildings include the optimal time to startup/shutdown the PGU and boiler, RES usage, charging/discharging state of a commercial-grade battery and the TES, amount of electricity flow from/to the power grid and related charging stations, and the amount of electricity and thermal energy charged, discharged, stored, and transmitted from/to any component of the system. Likewise, the hourly operational decisions of the charging stations include electricity flow from/to the power grid and related buildings, RES usage, V2G power usage, and battery management decisions (e.g., number of batteries charged, discharged, swapped, and stored). To alleviate the computational complexity associated with handing large number of scenarios, we employ a customized solution approach commonly known as the Sample Average Approximation (SAA) method. Computational results indicate that the SAA method is capable of producing high-quality solutions consistently

Table 5
Percentage changes in utilized resources at a commercial building and an EV charging station under different power grid disruption scenarios.

Scenario	Commercial building					EV charging station			
	PG (%)	PGU (%)	RES (%)	Battery (%)	CS (%)	PG (%)	V2G (%)	RES (%)	Building (%)
1	−17.69	11.57	−0.52	18.65	2.68	−19.83	10.35	−0.47	8.91
2	−20.22	12.17	0.78	19.65	3.14	−21.98	11.35	0.33	8.52
3	−11.24	9.63	0.46	15.67	3.15	−7.65	4.82	0.67	5.64
4	−5.75	7.68	0.25	9.68	2.98	−5.69	3.12	0.32	4.37
5	−24.89	14.74	0.16	22.52	3.03	−21.23	11.21	0.63	7.25
6	−21.53	13.54	0.67	20.68	3.87	−22.93	12.67	0.84	8.62

to realistic large-size problem instances within reasonable computational times. Finally, we use San Francisco as a test bed to visualize and validate the modeling results. A number of managerial insights are drawn, such as the impact of demand variability, power transaction limit, power grid disruption, and renewable resource size on the overall energy network cost and design.

The sensitivity analysis on parameters provide the following managerial insights for practitioners: (i) The overall energy network cost is increased by 14.24% when no energy collaboration is permitted between related commercial buildings and EV charging stations; (ii) A high level of demand variation on a commercial building leads to more energy storage in the commercial-grade battery and TES while less electricity flow to the power grid and associated EV charging stations. Likewise, a high level of demand variation on an EV charging station may lead to less electricity flow to the power grid and related commercial buildings while higher number of stored batteries and vice versa; (iii) During power grid disruption, charging stations rely more on commercial buildings than vice versa; (iv) The RES is already utilized almost on its maximum capacity; (v) The overall system cost is highly sensitive to the changes in RES sizes and the existence of collaboration between the commercial buildings and EV charging stations.

To summarize, the key contributions of this research to the existing literature are as follows: (i) proposing a novel collaborative decision model to study energy sharing among a cluster of commercial buildings and EV charging stations; (ii) modeling and realistically capturing different operational constraints that exist between multiple commercial buildings and EV charging stations; (iii) developing and testing a customized solution approach to solve the optimization model in a realistic-size network design problems; and (vi) developing a real-life case study based on the data from San Francisco, California. We believe the proposed optimization framework and managerial insights obtained from this study will help decision makers to design an efficient collaborative scheme between the charging stations and commercial buildings.

This research can be extended in several directions. A first would be to include consideration of the impact of EV congestion at the charging stations. Next, prevention and disruption models can be surveyed with respect to limited power grid utilization. Finally, it would be interesting to see how the stochastic nature of other parameters (e.g., renewable energy availability, state-of-charge for the batteries) impact the proposed collaboration scheme. These issues will be examined in future studies.

References

[1] U.S. Energy Information Administration. Energy consumption estimates by sector; 2017. Available from: < https://www.eia.gov/consumption/ > .

[2] U.S. Energy Information Administration. U.S. CO_2 emissions by sector; 2017. Available from: < http://architecture2030.org/buildings_problem_why/ > .

[3] Tasdighi M, Ghasemi H, Rahimi-Kian A. Residential microgrid scheduling based on smart meters data and temperature dependent thermal load modeling. IEEE Trans Smart Grid 2014;5(1):349–57.

[4] Rahmani-Andebili M, Shen H. Cooperative distributed energy scheduling for smart homes applying stochastic model predictive control. In: 2017 IEEE international conference on communications (ICC); 2017. p. 1–6.

[5] Rahmani-Andebili M, Shen H. Price-controlled energy management of smart homes for maximizing profit of a GENCO. IEEE Trans Syst, Man, Cybernet: Syst 2017.

[6] International Energy Agency (IEA). Global EV outlook 2017; 2017. Available from: < https://www.iea.org/publications/freepublications/publication/GlobalEVOutlook2017.pdf > .

[7] Liu C, Wang J, Botterud A, Zhou Y, Vyas A. Assessment of impacts of PHEV charging patterns on wind-thermal scheduling by stochastic unit commitment. IEEE Trans Smart Grid 2012;3(2)::675–683.

[8] Marmaras C, Xydas E, Cipcigan L. Simulation of electric vehicle driver behaviour in road transport and electric power networks. Transport Res Part C: Emerg Technol 2017;80:239–56.

[9] He Y, Venkatesh B, Guan L. Optimal scheduling for charging and discharging of electric vehicles. IEEE Trans Smart Grid 2012;3(3):1095–105.

[10] Ortega-Vazquez MA, Bouffard F, Silva V. Electric vehicle aggregator system operator coordination for charging scheduling and services procurement. IEEE Trans Power Syst 2013;28(2):1806–15.

[11] Haddadian G, Khalili N, Khodayar M, Shahiedehpour M. Security-constrained power generation scheduling with thermal generating units, variable energy resources, and electric vehicle storage for V2G deployment. Int J Electr Power Energy Syst 2015;73:498–507.

[12] Haddadian G, Khalili N, Khodayar M, Shahidehpour M. Optimal coordination of variable renewable resources and electric vehicles as distributed storage for energy sustainability. Sustain Energy, Grids Networks 2016;6:14–24.

[13] Fathabadi H. Utilization of electric vehicles and renewable energy sources used as distributed generators for improving characteristics of electric power distribution systems. Energy 2015;90:1100–10.

[14] Thomas D, Deblecker O, Ioakimidis CS. Optimal operation of an energy management system for a grid-connected smart building considering photovoltaics uncertainty and stochastic electric vehicles driving schedule. Appl Energy 2018;210:1188–206.

[15] DeForest N, MacDonald JS, Black DR. Day ahead optimization of an electric vehicle fleet providing ancillary services in the Los Angeles Air Force Base vehicle-to-grid demonstration. Appl Energy 2018;210:987–1001.

[16] Jin C, Sheng X, Ghosh P. Optimized electric vehicle charging with intermittent renewable energy sources. IEEE J Sel Top Signal Process 2014;8(6):1063–72.

[17] Hong L, Pingliang Z, Jianyi G, Huiyu W, Shaoyun G. An optimization strategy of controlled electric vehicle charging considering demand side response and regional wind and photovoltaic. J Modern Power Syst Clean Energy 2015;2(2):232–9.

[18] Rahmani-Andebili M, Fotuhi-Firuzabad M. An adaptive approach for PEVs charging management and reconfiguration of electrical distribution system penetrated by renewables. IEEE Trans Ind Inform 2018;14(5):2001–10.

[19] Zhang T, Chen W, Han Z, Cao Z. Charging scheduling of electric vehicles with local renewable energy under uncertain electric vehicle arrival and grid power price. IEEE Trans Veh Technol 2014;63(6):2600–12.

[20] Pan F, Bent R, Berscheid A, Izraelevitz D. Locating phev exchange stations in v2g. In: 2010 First IEEE international conference on smart grid communications; 2010. p. 173–8.

[21] Worley O, Klabjan D. Optimization of battery charging and purchasing at electric vehicle battery swap stations. In: 2011 IEEE vehicle power and propulsion conference; 2011. p. 1–4.

[22] Mak HY, Rong Y, Shen ZM. Infrastructure planning for electric vehicles with battery swapping. Manage Sci 2013;59(7):1557–75.

[23] Nurre SG, Bent R, Pan F, Sharkey TC. Managing operations of plug-in hybrid electric vehicle (PHEV) exchange stations for use with a smart grid. Energy Policy 2014;67:364–77.

[24] Liu N, Chen Z, Liu J, Tang X, Xiao X, Zhang J. Multi-objective optimization for component capacity of the photovoltaic-based battery switch stations: towards benefits of economy and environment. Energy 2014;64:779–92.

[25] Liu W, Niu S, Xu H, Li X. A new method to plan the capacity and location of battery swapping station for electric vehicle considering demand side management. Sustainability 2016;8(6):557.

[26] Widrick RS, Nurre SG, Robbins MJ. Optimal policies for the management of an electric vehicle battery swap station. Transport Sci 2016.

[27] Flores RJ, Shaffer BP, Brouwer J. Electricity costs for a Level 3 electric vehicle fueling station integrated with a building. Appl Energy 2017;191:367–84.

[28] Karan E, Mohammadpour A, Asadi S. Integrating building and transportation energy use to design a comprehensive greenhouse gas mitigation strategy. Appl Energy 2016;165:234–43.

[29] Clarke AD, Makram EB. A comprehensive analysis of plug in hybrid electric vehicles to commercial campus (V2C). Appl Energy 2015;3(01):24.

[30] Stadler M, Kloess M, Groissbock M, Cardoso G, Sharma R, Bozchalui MC, et al. Electric storage in Californias commercial buildings. Appl Energy 2013;104:711–22.

[31] Pang C, Dutta P, Kezunovic M. BEVs/PHEVs as dispersed energy storage for V2B uses in the smart grid. IEEE Trans Smart Grid 2012;3(1):473–82.

[32] Su W, Eichi H, Zeng W, Chow MY. A survey on the electrification of transportation in a smart grid environment. IEEE Trans Ind Inform 2012;8(1):1–10.

[33] Gough R, Dickerson C, Rowley P, Walsh C. Vehicle-to-grid feasibility: a techno-economic analysis of EV-based energy storage. Appl Energy 2017;192:12–23.

[34] Sehar F, Pipattanasomporn M, Rahman S. Demand management to mitigate impacts of plug-in electric vehicle fast charge in buildings with renewables. Energy 2017;120:642–51.

[35] Liu N, Chen Q, Liu J, Lu X, Li P, Lei J, et al. A heuristic operation strategy for commercial building microgrids containing EVs and PV system. IEEE Trans Ind Electron 2015;62(4):2560–70.

[36] Erdinc O. Economic impacts of small-scale own generating and storage units, and electric vehicles under different demand response strategies for smart households. Appl Energy 2014;126:142–50.

[37] Kuang Y, Chen Y, Hu M, Yang D. Influence analysis of driver behavior and building category on economic performance of electric vehicle to grid and building integration. Appl Energy 2017;207:427–37.

[38] Umetani S, Fukushima Y, Morita H. A linear programming based heuristic algorithm for charge and discharge scheduling of electric vehicles in a building energy management system. Omega 2017;67:115–22.

[39] Aziz M, Oda T, Kashiwagi T. Extended utilization of electric vehicles and their re-used batteries to support the building energy management system. Energy Procedia 2015;75:1938–43.

[40] Robledo CB, Oldenbroek V, Abbruzzese F, van Wijk AJ. Integrating a hydrogen fuel cell electric vehicle with vehicle-to-grid technology, photovoltaic power and a residential building. Appl Energy 2018;215:615–29.

[41] Rahmani-Andebili M, Shen H, Fotuhi-Firuzabad M. Planning and operation of parking lots considering system, traffic, and drivers behavioral model. IEEE Trans Syst, Man, Cybernet: Syst 2018.

[42] Rahmani-Andebili M, Venayagamoorthy GK. SmartPark placement and operation for improving system reliability and market participation. Electr Power Syst Res 2015;123:21–30.
[43] Chung SH, Kwon C. Multi-period planning for electric car charging station locations: a case of Korean Expressways. Eur J Oper Res 2015;242(2):677–87.
[44] Quddus MA, Hossain NUI, Marufuzzaman M, Jaradat RM, Roni MS. Sustainable network design for multi-purpose pellet processing depots under biomass supply uncertainty. Comput Ind Eng 2017;110:462–83.
[45] Quddus MA, Chowdhury S, Marufuzzaman M, Yu F, Bian L. A two-stage chance-constrained stochastic programming model for a bio-fuel supply chain network. Int J Prod Econ 2018;195:27–44.
[46] Poudel SR, Quddus MA, Marufuzzaman M, Bian L, Reuben FBV. Managing congestion in a multi-modal transportation network under biomass supply uncertainty. Ann Oper Res 2017:1–43.
[47] Marino C, Quddus MA, Marufuzzaman M, Cowan M, Bednar AE. A chance-constrained two-stage stochastic programming model for reliable microgrid operations under power demand uncertainty. Sustain Energy, Grids Networks 2018;13:66–77.
[48] Santoso T, Ahmed S, Goetschalckx M, Shapiro A. A stochastic programming approach for supply chain network design under uncertainty. Eur J Oper Res 2005;167:96–115.
[49] Kleywegt AJ, Shapiro A, Homem-De-Mello T. The sample average approximation method for stochastic discrete optimization. SIAM J Optim 2001;12:479–502.
[50] Mak WK, Morton DP, Wood RK. Monte Carlo bounding techniques for determining solution quality in stochastic programs. Oper Res Lett 1999;24:47–56.
[51] Norkin VI, Ermoliev YM, Ruszczynski A. On optimal allocation of indivisibles under uncertainty. Oper Res 1998;46:381–95.
[52] Norkin VI, Pflug GC, Ruszczynski A. A branch and bound method for stochastic global optimization. Math Programm 1998;83(3):425–50.
[53] General Algebraic Modeling System (GAMS); 2013. Available from: < http://www.gams.com/ > .
[54] FleetCarma. Comparing the Top 10 cities for electric vehicle adoption; 2016. Available from: < https://www.fleetcarma.com/top-cities-electric-vehicle-sales/ > .
[55] PlugShare. PlugShare EV Charging Station Map Find a place to charge your car; 2016. Available from: < https://www.plugshare.com/ > .
[56] National Renewable Energy Laboratory. National solar radiation data base; 2010. Available from: < http://rredc.nrel.gov/solar/old_data/nsrdb/ > .
[57] Salt River Project power and water. Electric vehicle price plan; 2015. Available from: < http://www.srpnet.com/prices/home/electricvehicle.aspx > .
[58] Plug in America. EV battery amortization costs and vehicle to grid; 2016. Available from: < http://pluginamerica.org/ev-battery-amortization-costs-and-vehicle-grid/ > .
[59] Sfexaminer. Electric cars in SF by the numbers; 2016. Available from: < http://www.sfexaminer.com/electric-cars-sf-numbers/ > .
[60] Gamou S, Yokoyama R, Ito K. Optimal unit sizing of cogeneration systems in consideration of uncertain energy demands as continuous random variables. Energy Convers Manage 2002;43(912):1349–61.